J|A|C|S

A R T I C L E S

Ligand-Directed Molecular Architectures: Self-Assembly of Two-Dimensional Rectangular Metallacycles and Three-Dimensional Trigonal or Tetragonal Prisms

Cheng-Yong Su,*,† Yue-Peng Cai,† Chun-Long Chen,† Mark D. Smith,§
Wolfgang Kaim,*,‡ and Hans-Conrad zur Loye*,§

*Contribution from the School of Chemistry and Chemical Engineering, Zhongshan University,
Guangzhou 510275, Peoples Republic of China, Institut für Anorganische Chemie, Universität
Stuttgart, Pfaffenwaldring 55, Stuttgart D-70569, Germany, and Department of Chemistry and
Biochemistry, The University of South Carolina, Columbia, South Carolina 29208*

Received January 21, 2003; E-mail: suchengyong1@yahoo.com; kaim@iac.uni-stuttgart.de; zurloye@mail.chem.sc.edu

Abstract: Three angular ditopic ligands (1,3-bis(benzimidazol-1-ylmethyl)-4,6-dimethylbenzene **L¹**, 1,3-bis(benzimidazol-1-ylmethyl)-2,4,6-trimethylbenzene **L²**, and 1,4-bis(benzimidazol-1-ylmethyl)-2,3,5,6-tetramethylbenzene **L³**) and one tripodal ligand 1,3,5-tris(benzimidazol-1-ylmethyl)-2,4,6-trimethylbenzene **L⁴** have been prepared. Reaction of these shape-specific designed ligands with different metal salts affords a series of discrete molecular architectures: $[Ag_2L^1{_2}](BF_4)_2$ **1**, $[Ag_2L^2{_2}](CF_3SO_3)_2$ **2**, $[CF_3SO_3^- \subset Ag_2L^3{_2}]$-$CF_3SO_3$ **3**, $[CF_3SO_3^- \subset Ag_2L^3{_3}]CF_3SO_3$ **4**, $[ClO_4^- \subset Cu_2L^4{_2}](ClO_4)_3$ **5**, $[4H_2O \subset Ni_2L^2{_4}Cl_4] \cdot 6H_2O$ **6**, $[BF_4^- \subset Ag_3L^4{_2}](BF_4)_2$ **7**, $[ClO_4^- \subset Ag_3L^4{_2}](ClO_4)_2$ **8**, and $[CuI_3{^{2-}} \subset Cu_3L^4{_2}]_2[Cu_2I_4]$ **9**. The compounds were characterized by elemental analysis, ESI-MS, IR, and NMR spectroscopy, and X-ray crystallography. **1** is a dinuclear metallacycle with 2-fold rotational symmetry in which two *syn*-conformational **L¹** ligands are connected by two linearly coordinated Ag⁺ ions. **2** and **3** are structurally related, consisting of rectangular structures assembled from two linearly coordinated Ag⁺ ions and two **L²** or **L³** ligands. The structure of **4** is a trigonal prismatic box consisting of two Ag⁺ ions in trigonal planar coordination linked by three **L³** ligands, while the structures of **5** and **6** are tetragonal prismatic cages constructed by two square planar Cu²⁺ or Ni²⁺ ions linked by four **L²** ligands. The topologies of **7**–**9** are similar to that of **4**; however, these three structures are assembled from three linearly coordinated Ag⁺ or Cu⁺ ions and two tripodal ligands, representing an alternative strategy to assembling a trigonal prism. ¹H NMR and ESI-MS were utilized to elucidate the solution structures of these macrocycles.

Introduction

The rapid development in the field of supramolecular chemistry has by now advanced to a stage where specified supramolecular structures can often be obtained by the assembly of judiciously selected building blocks under controlled reaction conditions. This permits the construction of well-defined supramolecular entities with intricate structures and potentially interesting functions.[1] Inorganic systems are particularly appealing because of the potential of incorporating a variety of desirable magnetic, electronic, optical, and catalytic properties.[2]

The self-assembly between specific metal centers and the selected ligands usually proceeds by the propagation of the steric and connectivity information stored in the organic ligands by

the metal ions via their local coordination geometries.[3] This type of synthetic strategy has proven to be quite effective in producing the desired products, in particular when compared to the alternative stepwise covalent synthetic approach. To date, research based on this approach has been extremely successful as evidenced by the many publications dealing with the assembly of diverse supramolecular constructs, such as linear and circular helicates,[4] interlocking rings,[5] molecular cages,[6] and one- to three-dimensional networks with fascinating structural topologies.[7]

Given the ready availability of different coordination modes provided by the plethora of metal cations available to chemists,

† Zhongshan University.
‡ Universität Stuttgart.
§ The University of South Carolina.

(1) (a) Lehn, J.-M. *Supramolecular Chemistry: Concepts and Perspectives*; VCH: Weinheim, 1995. (b) Lehn, J.-M. *Comprehensive Supramolecular Chemistry*; Pergamon Press: Oxford, 1996. (c) Desiraju, G. R. *Angew. Chem., Int. Ed. Engl.* **1995**, *34*, 2311. (d) Desiraju, G. R. *Nature* **2001**, *412*, 397. (e) Philp, D.; Stoddart, J. F. *Angew. Chem., Int. Ed. Engl.* **1996**, *35*, 1154. (f) Zaworotko, M. J. *Angew. Chem., Int. Ed.* **2000**, *39*, 17. (g) MacGillivray, L. R.; Atwood, J. L. *Nature* **1997**, *389*, 469. (h) Lehn, J.-M. *Chem.—Eur. J.* **2000**, *6*, 2097. (i) Mazik, M.; Bläser, D.; Boese, R. *Chem.—Eur. J.* **2000**, *6*, 2865.

(2) (a) Gardner, B.; Venkataraman, D.; Moore, J. S.; Lee, S. *Nature* **1995**, *374*, 792. (b) Yaghi, O. M.; Li, G.; Li, H. *Nature* **1995**, *378*, 703. (c) Li, H.; Laine, A.; O'Keeffe, M.; Yaghi, O. M. *Science* **1999**, *283*, 1145. (d) Li, H.; Eddaoudi, M.; O'Keeffe, M.; Yaghi, O. M. *Nature* **1999**, *402*, 276. (e) van Nostrum, C. F.; Picken, S. J.; Schouten, A.-J.; Nolte, R. J. M. *J. Am. Chem. Soc.* **1994**, *116*, 6089. (f) Zaworotko, M. J. *Angew. Chem., Int. Ed.* **1998**, *37*, 1211. (g) Linton, B.; Hamilton, A. D. *Chem. Rev.* **1997**, *97*, 1669. (h) Constable, E. C. *Chem. Commun.* **1997**, 1073. (i) Olenyuk, B.; Fechtenkötter, A.; Stang, P. J. *J. Chem. Soc., Dalton Trans.* **1998**, 1707. (j) Braga, D. *J. Chem. Soc., Dalton Trans.* **2000**, 3705.

(3) (a) Baxter, P. N. W.; Lehn, J.-M.; DeCian, A.; Fischer, J. *Angew. Chem., Int. Ed. Engl.* **1993**, *32*, 69. (b) Baxter, P. N. W.; Lehn, J.-M.; Kneisel, B. O.; Baum, G.; Fenske, D. *Chem.—Eur. J.* **1999**, *5*, 113. (c) Funeriu, D. P.; Lehn, J.-M.; Fromm, K. M.; Fenske, D. *Chem.—Eur. J.* **2000**, *6*, 2103.
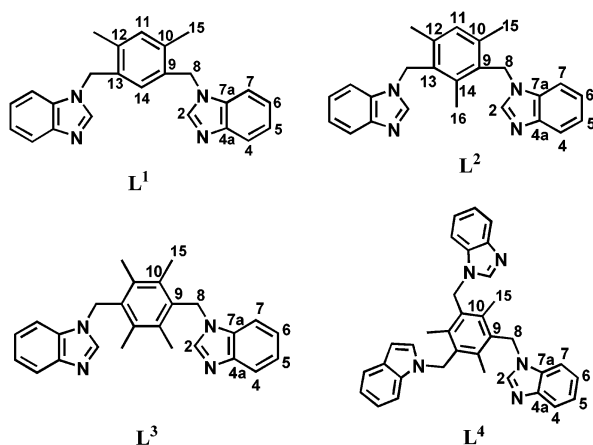
current research directions have increasingly focused on the design and synthesis of tailored organic ligands favoring structure-specific self-assembly. This is especially true in the field of metallacycles, where closed two- or three-dimensional structures can be formed by the coordination of selected metal ions with carefully chosen ligands.[8] A number of well-characterized discrete molecular aggregates with defined size and shape have been constructed, including many that have nanoscale dimensions.[9] Up to now, the most frequently prepared species were those having high symmetry, for example, two-dimensional (2D) polygonal macrocycles (molecular triangles, squares, pentagons, and hexagons) and three-dimensional (3D) polyhedral boxes (tetrahedral, hexagonal, cuboidal, adamantoid, and dodecahedral).[6,8,9] By comparison, relatively simple and low-symmetry species such as 2D rectangular-shaped molecules or 3D prismatic cage-shaped molecular structures have remained rare, although such lower-symmetry hosts can be expected to show desirable guest selectivity.[10] Furthermore, despite the continuous endeavor to elucidate the principles governing the formation of specific supramolecular aggregates, the achievement of control over the actual synthetic pathways needed for the rational design of discrete molecular architectures remains a great challenge.[8a,11] Although the metal ion coordination preference and the shape and bonding mode of the ligand are generally the primary considerations in metal-mediated self-assembly reactions, numerous other factors such as solvent,[12a,b] concentration,[12c,d] counterion,[12e] and even temperature[12f] may play a profound role in the formation of the thermodynamically (or kinetically) favored products. Interestingly, the silver(I) ion has been extensively employed in the assembly of a large number of diverse coordination polymers.[7b,r] While its coordination sphere is flexible (and hence less predictable) which can thus result in intricate coordination architectures,[12f,13] this same flexibility also affords an opportunity to investigate how the self-assembly process is influenced by modifications of the ligand denticity, the ligand-to-metal ratio, the counterions, and any noncovalent interactions.[13] It is reasonable that understanding and insight into the self-assembly process can be obtained by carrying out a systematic study using a series of soluble complexes assembled from geometrically similar ligands and coordination environment-flexible metal cations.

Our previous work has indicated that the tripodal ligand tris-(2-benzimidazolylmethyl)amine (ntb) and its derivatives with tertiary nitrogen binding sites is apt to bond with one or more metal ions to form discrete molecules or extended coordination structures possessing potential hydrogen-bonding donor sites ready for further assembly into multidimensional networks.[14] Similarly, linear quinoline-based polydentate ligands with flexible oligoglycol bridges will readily bind to one or more metal ions to yield metallamacrocyclic boxes or anion templated 2D arrays.[15] As expected, both types of ligands were able to form discrete structures; however, they did not form the desired high symmetry constructs.[8] Consequently, in a continuing effort

(4) (a) Albrecht, M. *Chem. Rev.* **2001**, *101*, 3407. (b) Piguet, C.; Bernardinelli, G.; Hopfgartner, G. *Chem. Rev.* **1997**, *97*, 2005. (c) Hasenknopf, B.; Lehn, J.-M.; Boumediene, N.; Dupont-Gervais, A.; Van Dorsselaer, A.; Kneisel, B.; Fensker, D. *J. Am. Chem. Soc.* **1997**, *119*, 10956. (d) Rice, C. R.; Wörl, S.; Jeffery, J. C.; Paul, R. L.; Ward, M. D. *Chem. Commun.* **2000**, 1529. (e) Hannon, M. J.; Painting, C. L.; Alcock, N. W. *Chem. Commun.* **1999**, 2023.

(5) (a) Fujita, M. *Acc. Chem. Res.* **1999**, *32*, 53. (b) Amabilino, D. B.; Stoddart, J. F. *Chem. Rev.* **1995**, *95*, 2725. (c) Weidmann, J.-L.; Kern, J.-M.; Sauvage, J.-P.; Muscat, D.; Mullins, S.; Köhler, W.; Rosenauer, C.; Räder, H. J.; Martin, K.; Geerts, Y. *Chem.—Eur. J.* **1999**, *5*, 1841. (d) Schill, G. *Catenane, Rotaxanes and Knots*; Academic Press: New York, 1971. (e) Constable, E. C.; Ward, M. D. *J. Am. Chem. Soc.* **1990**, *112*, 1256. (f) Amabilino, D. B.; Dietrich-Buchecker, C. O.; Sauvage, J.-P. *J. Am. Chem. Soc.* **1996**, *118*, 3285. (g) Whang, D.; Kim, K. *J. Am. Chem. Soc.* **1997**, *119*, 451. (h) Carlucci, L.; Ciani, G.; Moret, M.; Proserpio, D. M.; Rizzato, S. *Angew. Chem., Int. Ed.* **2000**, *39*, 1506. (i) Hoskins, B. F.; Robson, R.; Slizys, D. A. *Angew. Chem., Int. Ed. Engl.* **1997**, *36*, 2336.

(6) (a) Swiegers, G. F.; Malefetse, T. J. *Chem. Rev.* **2000**, *100*, 3483. (b) Saalfrank, R. W.; Uller, E.; Demleitner, B.; Bernt, I. *Struct. Bonding* **2000**, *96*, 149. (c) Caulder, D. L.; Raymond, K. N. *Acc. Chem. Res.* **1999**, *32*, 975. (d) Morgan, M.; Rebek, J., Jr. *Chem. Rev.* **1997**, *97*, 1647. (e) Jones, C. J. *Chem. Soc. Rev.* **1998**, *27*, 289. (f) Fujita, M. *Chem. Soc. Rev.* **1998**, *27*, 417. (g) Jacopozzi, P.; Dalcanale, E. *Angew. Chem., Int. Ed. Engl.* **1997**, *36*, 613. (h) Albrecht, M.; Röttele, H.; Burger, P. *Chem.—Eur. J.* **1996**, *2*, 1264.

(7) (a) Eddaoudi, M.; Moler, D. B.; Li, H.; Chen, B.; Reineke, T. M.; O'Keefee, M.; Yaghi, O. M. *Acc. Chem. Res.* **2001**, *34*, 319. (b) Blake, A. J.; Champness, N. R.; Hubberstey, P.; Li, W.-S.; Withersby, M. A.; Schröder, M. *Coord. Chem. Rev.* **1999**, *183*, 138. (c) Batten, S. R.; Robson, R. *Angew. Chem., Int. Ed.* **1998**, *37*, 1461. (d) Brunet, P.; Simard, M.; Wuest, J. D. *J. Am. Chem. Soc.* **1997**, *119*, 2737. (e) Ball, P. *Nature* **1996**, *381*, 648. (f) Carlucci, L.; Ciani, G.; Moret, M.; Proserpio, D. M.; Rizzato, S. *Chem. Mater.* **2002**, *14*, 12. (g) Bertelli, M.; Carlucci, L.; Ciani, G.; Proserpio, D. M.; Sironi, A. *J. Mater. Chem.* **1997**, *7*, 1271. (h) Yaghi, O. M.; Li, H.; Groy, T. L. *J. Am. Chem. Soc.* **1996**, *118*, 9096. (i) Copp, S. B.; Subramanian, S.; Zaworotko, M. J. *Angew. Chem., Int. Ed. Engl.* **1993**, *32*, 706. (j) Noro, S.-i.; Kitagawa, S.; Kondo, M.; Seki, K. *Angew. Chem., Int. Ed.* **2000**, *39*, 2081. (k) Kondo, M.; Shimamura, M.; Noro, S.-i.; Minakoshi, S.; Asami, A.; Seki, K.; Kitagawa, S. *Chem. Mater.* **2000**, *12*, 1288. (l) Ayyappan, P.; Evans, O. R.; Lin, W. *Inorg. Chem.* **2002**, *41*, 3328. (m) Evans, O. R.; Lin, W. *Inorg. Chem.* **1999**, *39*, 2189. (n) Dong, Y.-B.; Smith, M. D.; zur Loye, H.-C. *Angew. Chem., Int. Ed.* **2000**, *39*, 4271. (o) Dong, Y.-B.; Smith, M. D.; zur Loye, H.-C. *Inorg. Chem.* **2000**, *39*, 4927. (p) Hagrman, D.; Hammond, R. P.; Haushalter, R.; Zubieta, J. *Chem. Mater.* **1998**, *10*, 2091. (q) Wang, Q.-M.; Guo, G.-C.; Mak, T. C. W. *Chem. Commun.* **1999**, 1849. (r) Khlobystov, A. N.; Blake, A. J.; Champness, N. R.; Lemenovskii, D. A.; Majouga, A. G.; Zyk, N. V.; Schröder, M. *Coord. Chem. Rev.* **2001**, *222*, 155. (s) Power, K. N.; Hennigar, T. L.; Zaworotko, M. J. *New. J. Chem.* **1998**, 177. (t) Yaghi, O. M.; Li, H. *J. Am. Chem. Soc.* **1996**, *118*, 295.

(8) (a) Leininger, S.; Olenyuk, B.; Stang, P. J. *Chem. Rev.* **2000**, *100*, 853. (b) Stang, P. J. *Chem.—Eur. J.* **1998**, *4*, 19. (c) Caulder, D. L.; Raymond, K. N. *J. Chem. Soc., Dalton Trans.* **1999**, 1185. (d) Holliday, B. J.; Mirkin, C. A. *Angew. Chem., Int. Ed.* **2001**, *40*, 2023. (e) Fujita, M.; Umemoto, K.; Yoshizawa, M.; Fujita, N.; Kusukawa, K.; Biradha, K. *Chem. Commun.* **2001**, 509.

(9) For example, see: (a) Olenyuk, B.; Whiteford, J. A.; Fechtenkötter, A.; Stang, P. J. *Nature* **1999**, *398*, 796. (b) Stang, P. J.; Olenyuk, B. *Organometallics* **1997**, *16*, 3094. (c) Takeda, N.; Umemoto, K.; Yamaguchi, K.; Fujita, M. *Nature* **1999**, *398*, 794. (d) Kusukawa, T.; Fujita, M. *Angew. Chem., Int. Ed.* **1998**, *37*, 3142. (e) Ibukuro, F.; Kusukawa, T.; Fujita, M. *J. Am. Chem. Soc.* **1998**, *120*, 8561. (f) Fujita, M.; Oguro, D.; Miyazawa, M.; Oka, H.; Yamaguchi, K.; Ogura, K. *Nature* **1995**, *378*, 469. (g) Abrahams, B. F.; Egan, S. J.; Robson, R. *J. Am. Chem. Soc.* **1999**, *121*, 3535. (h) Scherer, M.; Caulder, D. L.; Johnson, D. W.; Raymond, K. N. *Angew. Chem., Int. Ed.* **1999**, *38*, 1587. (i) Kobayashi, K.; Shirasaka, T.; Yamaguchi, K.; Sakamoto, S.; Horn, E.; Furukawa, N. *Chem. Commun.* **2000**, 41. (j) Schnebeck, R.-D.; Freisinger, E.; Lippert, B. *Angew. Chem., Int. Ed.* **1999**, *38*, 168. (k) Colquhoun, H. M.; Fairman, R. A.; Tootell, P.; Williams, D. J. *J. Chem. Soc, Dalton Trans.* **1999**, 2651. (l) Hong, M.; Zhao, Y.; Su, W.; Cao, R.; Fujita, M.; Zhou, Z.; Chan, A. S. C. *J. Am. Chem. Soc.* **2000**, *122*, 4819.

(10) Kuehl, C. J.; Huang, S. D.; Stang, P. J. *J. Am. Chem. Soc.* **2001**, *123*, 9634.

(11) Levin, M. D.; Stang, P. J. *J. Am. Chem. Soc.* **2000**, *122*, 7428.

(12) (a) Baxter, P. N. W.; Khoury, R. G.; Lehn, J.-M.; Baum, G.; Fenske, D. *Chem.—Eur. J.* **2000**, *6*, 4140. (b) Long, D.-L.; Blake, A. J.; Champness, N. R.; Wilson, C.; Schröder, M. *Chem.—Eur. J.* **2002**, *8*, 2026. (c) Provent, C.; Rivara-Minten, E.; Hewage, S.; Brunner, G.; Williams, A. F. *Chem.—Eur. J.* **1999**, *5*, 3487. (d) Baum, G.; Constable, E. C.; Fenske, D.; Housecroft, C. E.; Kulke, T. *Chem. Commun.* **1999**, 195. (e) Caulder, D. L.; Powers, R. E.; Parac, T. N.; Raymond, K. N. *Angew. Chem., Int. Ed.* **1998**, *37*, 1840. (f) Baxter, P. N. W.; Lehn, J.-M.; Baum, G.; Fenske, D. *Chem.—Eur. J.* **2000**, *6*, 4510.

(13) (a) Toyota, S.; Woods, C. R.; Benaglia, M.; Haldimann, R.; Wärnmark, K.; Hardcastle, K.; Siegel, J. S. *Angew. Chem., Int. Ed.* **2001**, *40*, 751. (b) Hiraoka, S.; Yi, T.; Shiro, M.; Shionoya, M. *J. Am. Chem. Soc.* **2002**, *124*, 14510.

(14) (a) Su, C.-Y.; Kang, B.-S.; Liu, H.-Q.; Wang, Q.-G.; Mak, T. C. W. *Chem. Commun.* **1998**, 1551. (b) Su, C.-Y.; Kang, B.-S.; Liu, H.-Q.; Wang, Q.-G.; Chen, Z.-N.; Lu, Z.-L.; Tong, Y.-X.; Mak, T. C. W. *Inorg. Chem.* **1999**, *38*, 1374. (c) Su, C.-Y.; Kang, B.-S.; Yang, Q.-C.; Mak, T. C. W. *J. Chem. Soc., Dalton Trans.* **2000**, 1857. (d) Su, C.-Y.; Kang, B.-S.; Yang, Q.-C.; Mak, T. C. W. *J. Chem. Soc., Dalton Trans.* **2000**, 1831. (e) Su, C.-Y.; Yang, X. P.; Kang, B.-S.; Mak, T. C. W. *Angew. Chem., Int. Ed.* **2001**, *40*, 1725.

(15) (a) Su, C.-Y.; Liao, S.; Zhu, H.-L.; Kang, B.-S.; Chen, X.-M.; Liu, H.-Q. *J. Chem. Soc., Dalton Trans.* **2000**, 1985. (b) Liao, S.; Su, C.-Y.; Yeung, C.-H.; Xu, A.-W.; Zhang, H.-X.; Liu, H.-Q. *Inorg. Chem. Commun.* **2000**, *3*, 405.
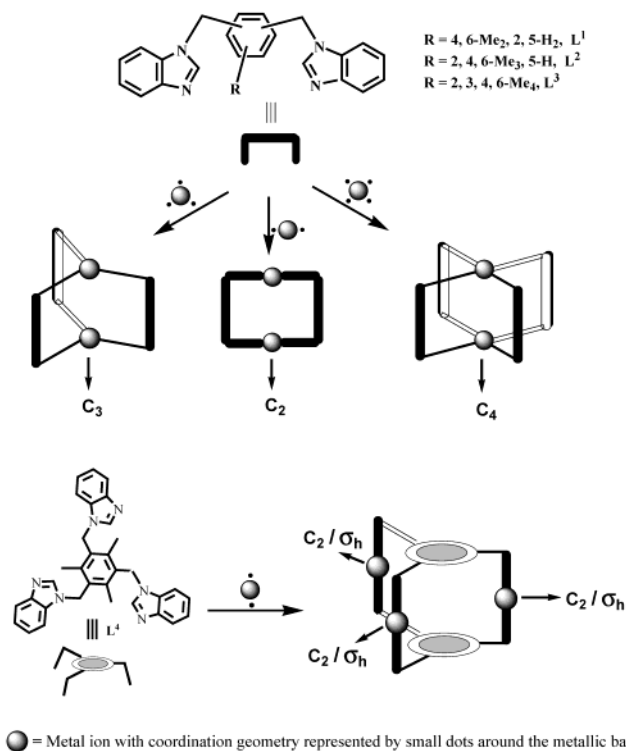
Scheme 1

Scheme 2

= Metal ion with coordination geometry represented by small dots around the metallic ball

to design suitable ligands capable of assembling preselected molecular architectures, we have prepared semirigid bi- and tridentate ligands constructed around central arene groups and extended with benzimidazolyl (Bim) arms (Scheme 1). Using these ligands, we were able to prepare model complexes with well-defined trigonal or tetragonal prismatic shapes that have been partially reported in preliminary communications.[16] In this paper, we describe the systematic design and syntheses of the ligands and their reactions to form a series of dinuclear rectangular-shaped macrocycles as well as trigonal or tetragonal prismatic 3D cages. Both the solid-state structures from X-ray crystallography and the solution dynamics as deduced from ^{1}H NMR and, indirectly, from ESI-MS are discussed.

Construction Approach. The synthetic strategies known as "Molecular Library Model" for molecular architectures or "Symmetry Interaction Model" for coordination clusters are well established.[8] The former relies principally on the combination of highly directional metal centers with specific open coordination sites and rigid, coordinatively inert di- or tritopic ligands with specific angles, whereas the latter is driven by the inherent symmetry of the coordination sites available at the metal centers, which are tethered by multibranched chelating ligands.[8] The rigid nature of nonchelating bi- and tridentate ligands accounts for the major reason beautiful canonical polygon or polyhedron structures have been obtained predominantly by the first strategy. In contrast, the relative flexibility of the ligands in the second strategy is a necessary requirement to enable the multiple chelation sites of the ligands to conform to the symmetry of the metal centers, yielding, for example, helical or tetrahedral clusters. In both cases, however, the simplest low-symmetry constructs, such as molecular rectangles or prisms, are not well represented in the literature.[8] One reason may be that suitable ligands with structures that would facilitate the formation of such molecules are not easily obtained. Recently, Stang and co-workers have proposed a *ligand-directed* approach by designing a molecular "clip": two parallel coordination sites are facing in the same direction, which allows for the assembly, for example, of a molecular rectangle (using rigid bipyridyl bridging ligands[10]) or of trigonal prisms (using tritopic ligands with pyridyl subunits).[17] In a similar approach, we have designed

a type of organic molecular "clip" that displays a coordination directing mode similar to Stang's organometallic clip (Scheme 1, **L$^{1-3}$**). In our case, two benzimidazole (Bim) rings were connected via methylene groups at the 1-position to an arene core to create a semirigid ligand possessing two arms that can rotate freely around the C—C bonds connecting them to the arene core. If two Bim rings take the *syn*-conformation,[18] then the two nitrogen donor atoms will point in the same direction, effectively converting the ligand to an organic clip (Scheme 2). Unlike the organometallic analogue, this type of organic clip contains two bulky arms that are available for binding to the metal ions which effectively defines the size of the resulting architectures. Consequently, the shape of the construct will be promoted by a combination of the coordination preference of the metal ions and the ligand shape.[12f,13] As indicated in Scheme 2, two linearly coordinating metal ions will connect two clips to form a rectangular-shaped structure, while two trigonally coordinating metal ions can lead to the formation of a trigonal prism; finally, a tetragonal prism may be generated by using two metal ions which prefer a square planar coordination environment. In other words, the shape of the molecular construct is driven by the preferred coordination between the metal ions and the ligands. On the other hand, if more than two arms are connected to the arene core and all of them are pointing in the same direction (*syn*-conformation),[18] then a 3D prismatic structure can be obtained. For example, two tripodal 1,3,5-tris(benzimidazol-1-ylmethyl)-2,4,6-trimethylbenzene ligands can be joined by three trigonal planar metal ions to form a trigonal prism with C_{3h} or even D_{3h} symmetry, as shown in

(16) (a) Su, C.-Y.; Cai, Y.-P.; Chen, C.-L.; Zhang, H.-X.; Kang, B.-S. *J. Chem. Soc., Dalton Trans.* **2001**, 359. (b) Su, C.-Y.; Cai, Y.-P.; Chen, C.-L.; Lissner, F.; Kang, B.-S.; Kaim, W. *Angew. Chem., Int. Ed.* **2002**, *41*, 3371.
(17) Kuehl, C. J.; Kryschenko, Y. K.; Radhakrishnan, U.; Seidel, S. R.; Huang, S. D. Stang, P. J. *Proc. Natl. Acad. Sci. U.S.A.* **2002**, *99*, 4932.

(18) Two predominant conformations are possible for all four ligands: if two Bim rings of **L^1**–**L^3** are located at the same side of the central arene core, the *syn*-conformation is assigned; otherwise, the *anti*-conformation is assigned. Similarly, the *syn*-conformation of **L^4** means all three arms are at the same side, while the *anti*-conformation means two on one side but the third at the opposite position.

Scheme 2. Consequently, by deliberately building a ligand that has two or more coordinative arms pointing in the same direction, we find the formation of 2D rectangular or 3D prismatic molecular architectures (depending on the metal ions) becomes easily achievable. The self-assembly of such architectures can be thought of as a *ligand-directed symmetry-interaction* model, although each arm of the ligand is monodentate and, in some cases, the axial positions of the metal ions are occupied by other small ligands.

Experimental Section

General Procedures. Commercially available reagents were used throughout without further purification; solvents were dried by standard procedures. 1,3-Bis(chloromethyl)-4,6-dimethylbenzene,[19] 1,3-bis(bromomethyl)-2,4,6-trimethylbenzene,[20] and 1,4-bis(bromomethyl)-2,3,5,6-tetramethylbenzene[20] were prepared according to the reported procedures. Infrared spectra were obtained from KBr pellets on a Perkin−Elmer 1600 Fourier Transform spectrometer in the 400−4000 cm^{-1} region. ^{1}H and ^{13}C NMR spectra were recorded on a Bruker 500 MHz DPX or a Bruker AC 250 spectrometer. All chemical shifts are reported in δ units with reference to the residual protons of the deuterated solvents or with respect to internal TMS (0.00 ppm). Elemental analyses (C, H, N) were performed on an Elemental Vario EL analytical instrument. ESI-MS was performed on a Micromass Q-tof or a Thermo Finigan LCQDECA XP ion trap mass spectrometer. The accelerating cone voltage was set as low as possible to minimize fragmentation processes.[21]

Syntheses. All ligands were typically prepared under argon by the following method: KOH was slowly added to a solution of benzimidazole in THF (50 mL) at room temperature with rigorous stirring. After about 4 h, a solution of the dibromo-, dichloro-, or tribromocompound in 50 mL of THF was added dropwise, and the reaction mixture was stirred continuously overnight. The solvent was subsequently removed under reduced pressure, and the residue was poured into 100 mL of water and extracted 3 times with dichloromethane (3 × 50 mL). The combined organic extracts were washed with water, dried (Na$_2$CO$_3$), and concentrated. The crude products were purified by recrystallization from hot ethanol or acetone to afford white crystalline solids.

1,3-Bis(benzimidazol-1-ylmethyl)-4,6-dimethylbenzene (L^1). Benzimidazole (4.72 g, 40 mmol), KOH (2.24 g, 40 mmol), and 1,3-bis-(chloromethyl)-4,6-dimethylbenzene (4.06 g, 20 mmol) were used as starting material. Yield: 1.73 g, 24%. ^{1}H NMR (DMSO-d_6) δ 8.148 (s, 2H, H2), 7.812 (dd, 2H, H4), 7.307 (m, 2H, H5), 7.254 (dd, 2H, H7), 7.175 (m, 2H, H6), 7.095 (s, 1H, H11), 6.725 (s, 1H, H14), 5.281 (s, 4H, H8), 2.256 (s, 4H, H15); ^{13}C NMR δ 142.51, 136.87, 133.82, 131.10, 128.68, 123.52, 122.86, 120.04, 109.96, 46.95, 18.69. IR (KBr, cm^{-1}) 3082(m), 1613(m), 1501(s), 1458(m), 1388(s), 1290(s), 1232(m), 1205(s), 1011(w), 915(w), 743(s), 618(w). Anal. Calcd for C$_{24}$H$_{22}$N$_4$: C, 78.66; H, 6.05; N, 15.29. Found: C, 78.26; H, 5.89; N, 15.55.

1,3-Bis(benzimidazol-1-ylmethyl)-2,4,6-trimethylbenzene (L^2). Benzimidazole (1.06 g, 9 mmol), KOH (1.00 g, 18 mmol), and 1,3-bis-(bromomethyl)-2,4,6-trimethylbenzene (1.377 g, 4.5 mmol) were used. Yield: 1.35 g, 81%. ^{1}H NMR (DMSO-d_6) δ 7.724 (s, 2H, H2), 7.637 (dd, 2H, H4), 7.439 (dd, 2H, H7), 7.198 (m, 4H, H5,6), 7.131 (s, 1H, H11), 5.418 (s, 4H, H8), 2.290 (s, 6H, H15), 2.162 (s, 3H, H16); ^{13}C NMR δ 140.97, 139.38, 138.30, 131.81, 128.91, 123.66, 123.19, 119.92, 109.77, 43.88, 20.00, 15.64. IR (KBr, cm^{-1}) 3049(m),

2968(w), 1610(m), 1494(s), 1453(m), 1385(m), 1323(m), 1283(m), 1249(m), 1202(s), 1007(w), 880(m), 743(s), 624(w), 427(m). Anal. Calcd for C$_{25}$H$_{24}$N$_4$: C, 78.95; H, 6.32; N, 14.74. Found: C, 78.89; H, 6.54; N, 15.03.

1,4-Bis(benzimidazol-1-ylmethyl)-2,3,5,6-tetramethylbenzene (L^3). Benzimidazole (1.06 g, 9 mmol), KOH (1.00 g, 18 mmol), and 1,4-bis(bromomethyl)-2,3,5,6-tetramethylbenzene benzene (1.44 g, 4.5 mmol) were used. Yield: 1.55 g, 87%. ^{1}H NMR (DMSO-d_6) δ 7.698 (s, 2H, H2), 7.655 (dd, 2H, H4), 7.605 (dd, 2H, H7), 7.276 (m, 2H, H5), 7.218 (m, 2H, H6), 5.491 (s, 4H, H8), 2.199 (s, 12H, H15). IR (KBr, cm^{-1}) 3086(m), 2915(w), 1613(m), 1497(s), 1455(m), 1383(m), 1323(m), 1283(m), 1238(m), 1204(s), 1007(w), 887(m), 740(s), 626(w), 429(m). Anal. Calcd for C$_{26}$H$_{26}$N$_4$: C, 79.19; H, 6.60; N, 14.21. Found: C, 79.01; H, 6.89; N, 14.49.

1,3,5-Tris(benzimidazol-1-ylmethyl)-2,4,6-trimethylbenzene (L^4). Benzimidazole (2.24 g, 18 mmol), KOH (1.12 g, 20 mmol), and 2,4,6-tris(bromomethyl)mesitylene (2.39 g, 6 mmol) were used. Yield: 2.2 g, 71%. ^{1}H NMR (DMSO-d_6) δ 7.867 (s, 3H, H2), 7.650 (dd, 3H, H4), 7.523 (dd, 3H, H7), 7.220 (m, 3H, H5), 7.202 (m, 3H, H6), 5.505 (s, 6H, H8). ^{13}C NMR δ 143.87, 141.08, 139.81, 133.85, 130.74, 123.38, 122.77, 120.64, 109.34, 44.15, 16.52. IR (KBr, cm^{-1}) 3053(w), 1611(m), 1496(s), 1456(s), 1386(m), 1323(m), 1284(m), 1227(m), 1205(m), 1032(w), 1007(w), 890(w), 746(s), 625(w), 575(w), 428(w). Anal. Calcd for C$_{33}$H$_{30}$N$_6$: C, 77.65; H, 5.88; N, 16.47. Found: C, 77.28; H, 5.54; N, 16.85.

[Ag$_2$L$^1_2$](BF$_4$)$_2$ 1. Silver tetrafluoroborate (0.019 g, 0.1 mmol) in 5 mL of methanol was added to a solution of L^1 (0.037 g, 0.1 mmol) in 2 mL of dichloromethane. The mixture was stirred at room temperature for 10 min, and the resulting precipitate was collected by filtration. Yield: 46%. ^{1}H NMR (DMSO-d_6) δ 8.369 (s, 2H, H2), 7.768 (dd, 2H, H4), 7.293 (dd, 2H, H7), 7.281 (m, 2H, H5), 7.155 (m, 3H, H6 and H11), 6.171 (s, 1H, H14), 5.488 (s, 4H, CH8), 2.290 (s, 6H, −CH$_3$). IR (KBr, cm^{-1}) 3115(w), 2924(w), 1658(w), 1616(m), 1513(s), 1462(m), 1388(m), 1298(w), 1270(m), 1057(vs), 743(s), 617(w), 427(w). Anal. Calcd for C$_{48}$H$_{44}$N$_8$B$_2$F$_8$Ag$_2$: C, 51.37; H, 3.95; N, 9.98. Found: C, 51.01; H, 3.97; N, 10.31. Single crystals suitable for X-ray analyses were obtained by slow diffusion of diethyl ether into the CH$_3$CN diluted reaction mixture, giving the formulation **1**·1.5CH$_3$CN.

[Ag$_2$L$^2_2$]$_2$(CF$_3$SO$_3$)$_2$ 2. A MeOH (10 mL) solution of L^2 (0.38 g, 1 mmol) was added to an MeCN (10 mL) solution of silver trifluoromethanesulfonate (0.26 g, 1 mmol). After filtration, the filtrate was left standing at ambient temperature to give colorless needle crystals upon slow evaporation of the solvent. Yield: 30%. ^{1}H NMR (DMSO-d_6) δ 8.046 (s, 2H, H2), 7.95−7.84 (m, 4H, H4,7), 7.35−7.52 (m, 4H, H5,6), 7.242 (s, 1H, H11), 5.584 (s, 4H, H8), 2.316 (s, 6H, H15), 2.153 (s, 3H, H16). IR (KBr, cm^{-1}) 3112(w), 2968(w), 2913(w), 1613(w), 1510(m), 1461(m), 1397(m), 1267(vs), 1234(m), 1155(m), 1026(s), 744(m), 632(m), 572(w), 516(w), 472(w), 426(w). Anal. Calcd for C$_{52}$H$_{48}$N$_8$F$_6$O$_6$S$_2$Ag$_2$: C, 48.98; H, 3.77; N, 8.79. Found: C, 49.42; H, 3.96; N, 8.82.

[Ag$_2$L$^3_2$](CF$_3$SO$_3$)$_2$ 3. A methanol solution (20 mL) of L^3 (0.39 g, 1 mmol) was slowly added to an MeCN (30 mL) solution of silver trifluoromethanesulfonate (0.26 g, 1 mmol). The resulting mixture was left standing at ambient temperature for several days to give colorless block crystals. Yield: 87%. ^{1}HNMR (DMSO-d_6) δ 8.005 (dd, 2H, H4), 7.897 (dd, 2H, H7), 7.853 (s, 2H, H2), 7.55−7.43 (m, 4H, H5,6), 5.625 (s, 4H, H8), 2.223 (s, 12H, H15). IR (KBr, cm^{-1}) 3113(w), 3046(w), 1619(w), 1430(m), 1252(vs), 1176(s), 1081(w), 1046(s), 808(m), 762(w), 638(s), 576(w), 518(m), 441(w). Anal. Calcd for C$_{54}$H$_{52}$N$_8$-F$_6$O$_6$S$_2$Ag$_2$: C, 49.77; H, 3.89; N, 8.62. Found: C, 49.53; H, 3.97; N, 8.98.

[Ag$_2$L$^3_3$](CF$_3$SO$_3$)$_2$ 4. Preparation of this complex was improved as follows:[16a] To an MeCN (10 mL) solution of silver trifluoromethanesulfonate (0.26 g, 1 mmol) was added a methanol solution (10 mL) of L^3 (0.59 g, 1.5 mmol). A colorless crystalline precipitate formed in a few minutes to which DMSO was added while heating until the solid

(19) Gerisch, M.; Krumper, J. R.; Bergman, R. G.; Tilley, R. G. *J. Am. Chem. Soc.* **2001**, *123*, 5816.
(20) van der Made, A. W.; van der Made, R. H. *J. Org. Chem.* **1993**, *58*, 1262−1263.
(21) (a) Marquis-Rigault, A.; Dupont-Gervais, A.; Baxter, P. N. W.; Dorsselaer, A. V.; Lehn, J.-M. *Inorg. Chem.* **1996**, *35*, 2307. (b) Bruins, A. P.; Covey, T. R.; Henion, J. D. *Anal. Chem.* **1987**, *59*, 2642.

disappeared and clear solution was obtained. The resulting mixture was left standing at ambient temperature for several days to give colorless hexagonal-shaped crystals. Yield: 72%. ^{1}H NMR (DMSO-d_6) δ 7.873 (dd, 2H, H4), 7.827 (s, 2H, H2), 7.819 (dd, 2H, H7), 7.44−7.38 (m, 4H, H5,6), 5.590 (s, 4H, H8), 2.220 (s, 12H, H15). For IR and elemental analysis results, see ref 16a.

[Cu$_2$L$^2_4$](ClO$_4$)$_4$ 5. See ref 16a.

[Ni$_2$L$^2_4$Cl$_4$]·10H$_2$O 6. The process was the same as that for **5** but used NiCl$_2$·6H$_2$O (0.23 g, 1 mmol) rather than Cu(ClO$_4$)$_2$·6H$_2$O as starting material. Yield: 80%. IR (KBr, cm^{-1}) 3384(br), 3270(s), 3078(m), 2969(w), 2916(w), 2865(w), 1612(m), 1524(m), 1462(m), 1402(m), 1325(w), 1296(m), 1240(m), 1189(m), 1014(w), 929(w), 742(m), 613(m), 478(w), 428(w). Anal. Calcd for C$_{100}$H$_{116}$N$_{16}$Cl$_4$-O$_{10}$Ni$_2$: C, 61.24; H, 5.96; N, 11.43. Found: C, 61.60; H, 5.82; N, 11.63.

[Ag$_3$L$^4_2$](BF$_4$)$_3$ 7. Preparation refers to ref 16b. IR (KBr, cm^{-1}) 3108(w), 2956(w), 2916(w), 1615(w), 1516(m), 1462(m), 1395(w), 1327(w), 1294(m), 1225(m), 1054(vs), 924(w), 743(m), 620(w), 426(w). The single crystals with the formulation of **7**·CH$_3$CN·H$_2$O suitable for X-ray analyses were obtained by slow diffusion of diethyl ether into the diluted reaction mixture.

[Ag$_3$L$^4_2$](ClO$_4$)$_3$ 8. The preparation was the same as that of **7** but used AgClO$_4$ instead of AgBF$_4$. Yield: 90%. ^{1}H NMR (DMSO-d_6) δ 8.112 (dd, 6H, H4), 8.072 (s, 6H, H2), 7.918 (dd, 6H, H7), 7.510 (m, 6H, H6), 7.451 (m, 6H, H5), 5.678 (s, 12H, H8), 2.467 (s, 18H, −CH$_3$). IR (KBr, cm^{-1}) 3116(w), 2971(w), 1660(w), 1614(w), 1515(m), 1462(m), 1395(m), 1295(m), 1225(m), 1087(vs), 922(w), 742(m), 622(m), 426(w). Anal. Calcd for C$_{66}$H$_{60}$N$_{12}$Cl$_3$O$_{12}$Ag$_3$: C, 48.24; H, 3.68; N, 10.23. Found: C, 48.32; H, 3.90; N, 10.60. Single crystals with the formulation of **8**·MeCN·0.5MeOH·0.25H$_2$O suitable for X-ray analyses were obtained by slow diffusion of diethyl ether into the diluted reaction mixture.

[Cu$_3$L$^4_2$·CuI$_3$]$_2$[Cu$_2$L$_4$] 9. Preparation refers to ref 16b. IR (KBr, cm^{-1}) 3107(w), 2963(w), 1667(w), 1614(w), 1510(m), 1460(m), 1391(m), 1290(m), 1220(m), 1195(m), 1007(w), 742(s), 619(w), 423(w). Single crystals suitable for X-ray analyses were obtained by slow evaporation of the reaction mixture diluted by DMF, giving the formulation of **9**·7H$_2$O. If a small portion of benzene is added to the reaction mixture during crystallization, a complex with the formulation of **9**·benzene·6H$_2$O is obtained.

Crystal Structure Determination. Intensity data for **1**·1.5CH$_3$CN and **9**·benzene·6H$_2$O were collected at −100 °C on a Siemens P4 four-circle diffractometer with graphite monochromated Mo Kα radiation (λ = 0.710 73 Å) using the ω−2θ scan technique. An empirical absorption correction based on ψ-scans of several reflections was applied. All other data were collected (hemisphere technique) on either a NONIUS Kappa or Bruker SMART 1K diffractometer with a CCD area detector using ω rotations, and absorption corrections were applied with the HABITUS or SADABS program.[22] All the structures were solved by direct methods and refined by full-matrix least-squares against F^2 of all data using the SHELXTL program package.[23] Anisotropical thermal factors were assigned to most of the nondisordered non-hydrogen atoms except those showing severe disorder as explained below. The positions of the hydrogen atoms were generated geometrically, assigned isotropic thermal parameters, and allowed to ride on their respective parent atoms before the final cycle of least-squares refinement.

Many anionic molecules were found to exhibit disorder related to the symmetry of the structures and were, consequently, symmetrically modeled. Two acetonitrile molecules in **1** occupy different special

positions: one on the *m* plane and another at the 4-fold axis with C2w atom locating at the 4/*m* position. Both of them are refined with fractional occupancies. In **3**, one CF$_3$SO$_3^-$ anion possesses a center of symmetry with *i* located in the middle of the C−S bond. The CF$_3$ group and the SO$_3$ group, consequently, occupy the same positions with the sum of site occupation factors equal to unity. Another one is disordered over two locations related by the inversion center in which three fluorine atoms are further disordered between two slightly different positions. The CF$_3$SO$_3^-$ anions in complex **4** show a similar disordered pattern; however, the first CF$_3$SO$_3^-$ anion possesses $\bar{3}$ symmetry with the inversion center lying in the middle of the C−S bond, while another was 3-fold orientationally disordered with one oxygen atom lying on the C_3 axis and a perpendicular symmetrical mirror passing through the C−S bond. The perchlorate anions in **5** show severe disorder. One perchlorate anion is located inside the molecular box with two oxygen atoms lying on the 4-fold axis and the other two oxygen atoms and the chlorine atom occupying the mirror plane. Thereby, four sets of ClO$_4^-$ groups are generated to share two oxygen atoms having 4-fold symmetry. The sum of the site occupancy of four 4/*m* symmetry-related ClO$_4^-$ groups amount to one. An additional perchlorate anion is disordered along the 4-fold axis outside the box. Two oxygen atoms are lying at the 4-fold axis, and the other two oxygen atoms occupy the mirror plane; however, the chlorine atom is not in a special position hence showing axial disorder in eight positions. The total occupancy factor of every atom adds up to one. The third ClO$_4^-$ is located on a center of symmetry but exhibits disorder over two closely adjacent locations with total occupancy factors equal to one. The forth perchlorate anion lies on the σ_h mirror. The four water molecules located in the molecular box of **6** are well ordered because of the formation of Cl⋯O hydrogen bonds; however, the ones outside the box show disorder related to the *m* or 4 symmetry. Only one of the three BF$_4^-$ groups in **7** is disordered with each fluorine atom occupying two sites and refined with half occupancy. The water molecule was split over four positions. The perchlorate anions in **8** exhibit the same disorder as that in **7**, but the methanol molecule has only half occupancy. All the water molecules in **9**·7H$_2$O and **9**·benzene·6H$_2$O are severely disordered and refined with fractional occupancies. The Cu$_2$L$_4^{2-}$ anion exhibits a *pseudo-C$_2$* axis along the Cu(10)−I(7) bond and shows disorder in that way. Because of weak diffraction, most of the C and N atoms in **9**·benzene·6H$_2$O were refined isotropically. A summary of the crystal data is given in Table 1. Selected bond distances and bond angles are listed in Table S1. Further details are presented in the Supporting Information.

Results and Discussion

Syntheses and Solid-State Structures. All four ligands can be conveniently prepared from the substitution reaction between 1*H*-benzimidazole and the respective bromide or chloride compounds under strong alkaline (KOH) conditions. The chemical composition and purity of the ligands were confirmed by NMR, IR, and elemental analyses. The solid-state structure of the ligand **L^4** shows that all three Bim arms are nearly perpendicular to the mesitylene core with two nitrogen donors pointing up and one down,[24] that is, exhibiting an *anti*-conformation.[18] In solution, it is expected that fast conformational exchange will take place because of low rotational energy barriers between the *anti*- and *syn*-conformations. An analogous process is expected for the bidentate ligands. The preparation of the complexes was readily achieved in one-pot reactions by combining the ligands with the respective metal salts in different metal-to-ligand ratios (Scheme 3). Elemental analyses of the

(22) Herrendorf, W. HABITUS: *Programm zur Optimierung der Kristallgestalt für die numerische Absorptionskorrektur.* Dissertation, Universität Karlsruhe, Germany, 1993. (b) Sheldrick, G. M. *ADABS: Program for scaling and correction of area detector data.* University of Göttingen: Germany, 1996.

(23) *SHELXTL, Version 5.10*; Bruker Analytical X-ray Systems: Madison, WI, 1998.

(24) Cai, Y.-P.; Kang, B.-S.; Su, C.-Y.; Zhang, H.-X.; Yang, X.-P.; Deng, L.-R.; Xu, A.-W.; Zhou, Z.-Y.; Chan, A. S. C. *Chin. J. Struct. Chem.* **2001**, *20*, 262.

Table 1. Crystal Data for **1**·1.5CH₃CN, **2**–**5**, **6**, **7**·CH₃CN·H₂O, **8**·MeCN·0.5MeOH·0.25H₂O, **9**·7H₂O and **9**·Benzene·6H₂O

	1·1.5CH₃CN	**2**	**3**	**4**	**5**
empirical formula	$C_{51}H_{48.5}Ag_2B_2F_8N_{9.5}$	$C_{52}H_{48}Ag_2F_6N_8O_6S_2$	$C_{54}H_{52}Ag_2F_6N_8O_6S_2$	$C_{80}H_{78}Ag_2F_6N_{12}O_6S_2$	$C_{100}H_{96}Cl_4Cu_2N_{16}O_{16}$
fw	1183.85	1274.84	1302.90	1697.40	2046.81
cryst syst	tetragonal	triclinic	triclinic	hexagonal	tetragonal
space group	*P*4/*mnc*	*P*1̄	*P*1̄	*P*6(3)/*m*	*I*4/*m*
a (Å)	18.555(3)	10.0439(12)	9.1423(6)	14.0129(13)	18.6162(11)
b (Å)	18.555(3)	11.5002(14)	11.4306(8)	14.0129(13)	18.6162(11)
c (Å)	15.958(3)	12.4933(16)	15.1363(16)	23.119(3)	16.1840(13)
α (deg)	90	63.602(2)	73.5910(10)	90	90
β (deg)	90	86.826(2)	75.0770(10)	90	90
γ (deg)	90	87.684(2)	74.3250(10)	120	90
V (Å³)	5494.0(15)	1290.4(3)	1432.53(17)	3931.5(7)	5608.8(7)
Z	4	1	1	2	2
ρ_{calc} (g cm⁻³)	1.431	1.641	1.510	1.434	1.212
T (K)	173(2)	293(2)	293(2)	293(2)	293(2)
μ (mm⁻¹)	0.783	0.920	0.831	0.625	0.539
GOF	0.989	1.000	1.013	1.050	1.136
*R*1[a]	0.0855	0.0515	0.0544	0.0716	0.1070
*wR*2[b]	0.2623	0.1068	0.1644	0.1935	0.2353

	6	**7**·CH₃CN·H₂O	**8**·MeCN·0.5MeOH·0.25H₂O	**9**·7H₂O	**9**·benzene·6H₂O
empirical formula	$C_{100}H_{116}Cl_4N_{16}Ni_2O_{10}$	$C_{68}H_{65}Ag_3B_3F_{12}N_{13}O$	$C_{68.5}H_{65.5}Ag_3Cl_3N_{13}O_{12.75}$	$C_{132}H_{144}Cu_{10}I_{10}N_{24}O_7$	$C_{138}H_{138}Cu_{10}I_{10}N_{24}O_6$
fw	1961.31	1664.37	1704.80	4083.11	4133.12
cryst syst	tetragonal	tetragonal	tetragonal	triclinic	monoclinic
space group	*I*4/*m*	*P*4(2)/*n*	*P*4(2)/*n*	*P*1̄	*P*2(1)/*n*
a (Å)	15.301(2)	27.824(4)	28.108(3)	16.935(3)	19.893(6)
b (Å)	15.301(2)	27.824(4)	28.108(3)	17.165(3)	40.398(13)
c (Å)	23.303(5)	18.108(4)	18.335(3)	30.625(6)	23.814(9)
α (deg)	90	90	90	101.72(3)	90
β (deg)	90	90	90	102.94(3)	108.19(2)
γ (deg)	90	90	90	91.36(3)	90
V (Å³)	5455.7(15)	14020(4)	14485(3)	8473(3)	18182(11)
Z	2	8	8	2	4
ρ_{calc} (g cm⁻³)	1.194	1.577	1.563	1.600	1.510
T (K)	293(2)	173(2)	293(2)	293(2)	293(2)
μ (mm⁻¹)	0.503	0.915	0.984	3.102	2.892
GOF	0.982	1.017	0.928	1.052	0.929
*R*1[a]	0.0798	0.0801	0.0643	0.0847	0.0817
*wR*2[b]	0.1981	0.1859	0.1573	0.2301	0.1726

[a] $R1 = \sum\{|F_o| - |F_c|\}/\sum|F_o|$. [b] $wR2 = [\sum w(F_o{}^2 - F_c{}^2)^2/\sum w(F_o{}^2)^2]^{1/2}$.

solid products led to the following stoichiometries for the nine complexes: AgL¹(BF₄) **1**, AgL²(CF₃SO₃) **2**, AgL³(CF₃SO₃) **3**, Ag₂L³₃(CF₃SO₃)₂ **4**, CuL²₂(ClO₄)₂ **5**, NiL²₂Cl₂(H₂O)₂ **6**, Ag₃L⁴₂-(BF₄)₃ **7**, Ag₃L⁴₂(ClO₄)₃ **8**, and Cu₅I₅L⁴₂ **9**. While the chemical composition, in particular the metal-to-ligand ratio of the products, can preclude, as well as sometimes suggest, certain structural arrangements, it is by no means sufficient for making any structural predictions due to the many different structural architectures of coordination frameworks that can be generated from identical stoichiometries. Therefore, single crystals of all the above compounds were grown to definitively establish their solid-state structure by X-ray diffraction. In several cases, some solvents molecules were found trapped within the crystal lattice; however, there is no indication that they significantly influence the product structure. This is especially true for the structures of **9**·7H₂O and **9**·benzene·6H₂O, where the cocrystallization of one benzene molecule altered the crystal system but left the M₃L₂ cage structure essentially intact (see below).

M₂L₂ Rectangular Metallacycles. X-ray diffraction analyses revealed that the complexes **1**–**3** form discrete metallacycles, consisting of two ligands and two metal ions, which represent the smallest 2D cyclic assembly possible for closed structures with a 1:1 metal-to-ligand ratio.

The crystal structure of **1** consists of a binuclear dicationic [Ag₂L¹₂]²⁺ motif, two BF₄⁻ anions, and 1.5 acetonitrile mole-

cules per formula unit. Two ligands are arranged in a face-to-face *syn*-conformation to coordinate to two Ag(I) ions from opposite directions, generating a locally linear geometry around the metal ions. The [Ag₂L¹₂]²⁺ cation has high symmetry. A mirror plane *m*, containing two unsubstituted carbon atoms of the benzene ring, divides the ligand into two equivalent parts, while a C_2 axis passes through the two Ag⁺ ions. Thus, a crystallographically imposed 2/*m* symmetry is located at the center of the cluster and generates the entire molecule from the asymmetric unit, containing only half of a ligand and one Ag⁺ ion. This leads to the formation of a typical rectangular cavity formed from two ligands and two Ag⁺ ions, as shown in Figure 1.

Compound **2** contains a similar four-membered [Ag₂L²₂]²⁺ cyclic motif; however, the two ligands are oriented in a head-to-head *syn*-conformation to bind two Ag⁺ ions that consequently protrude toward the inside and generate a somewhat bent coordination geometry.[25] In contrast to the structure of **1**, there is only an inversion center *i* in the molecule without any crystallographically imposed symmetry for the ligand or the metal ions. However, the two ligands are arranged in such a way that a *pseudo-C₂* axis can be imagined to run through the two Ag⁺ ions. That is, a rotation of 180° along the Ag···Ag

(25) Su, C.-Y.; Kang, B.-S.; Du, C.-X.; Yang, Q.-C.; Mak, T. C. W. *Inorg. Chem.* **2000**, *39*, 4843.
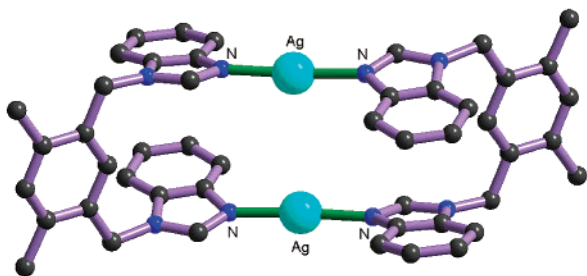
Figure 1. Ball and stick representation of the $[Ag_2L^1_2]^{2+}$ cation in **1**·1.5CH$_3$CN.

axis can generate one ligand from the other. The rectangular shape is more apparent in comparison to **1**, and the cavity enclosure is completed by two parallel basal mesitylene rings pointing in opposite directions (Figure 2). One CF$_3$SO$_3^-$ anion is dangling above each mesitylene ring on both sides of the molecule with an Ag···O interaction of 2.613 Å.

Compound **3** shows the most regular rectangular structure, although it only possesses real *i* symmetry in the molecular center. Nonetheless, a straight head-to-head arrangement of two 1,4-substituted Bim arms generates a *pseudo*-2-fold symmetry
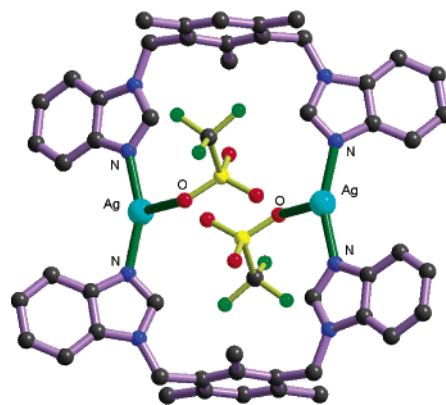
Figure 2. Ball and stick representation of the crystal structure of **2** showing two dangling CF$_3$SO$_3^-$ anions.

along the Ag···Ag axis and a *pseudo*-mirror symmetry through the four coplanar Bim rings attached to the two different ligands. The cavity formed between two exactly parallel durene rings accommodates a disordered CF$_3$SO$_3^-$ anion whose oxygen atoms weakly interact with the Ag$^+$ ions at ca. 2.75 Å, as

Scheme 3
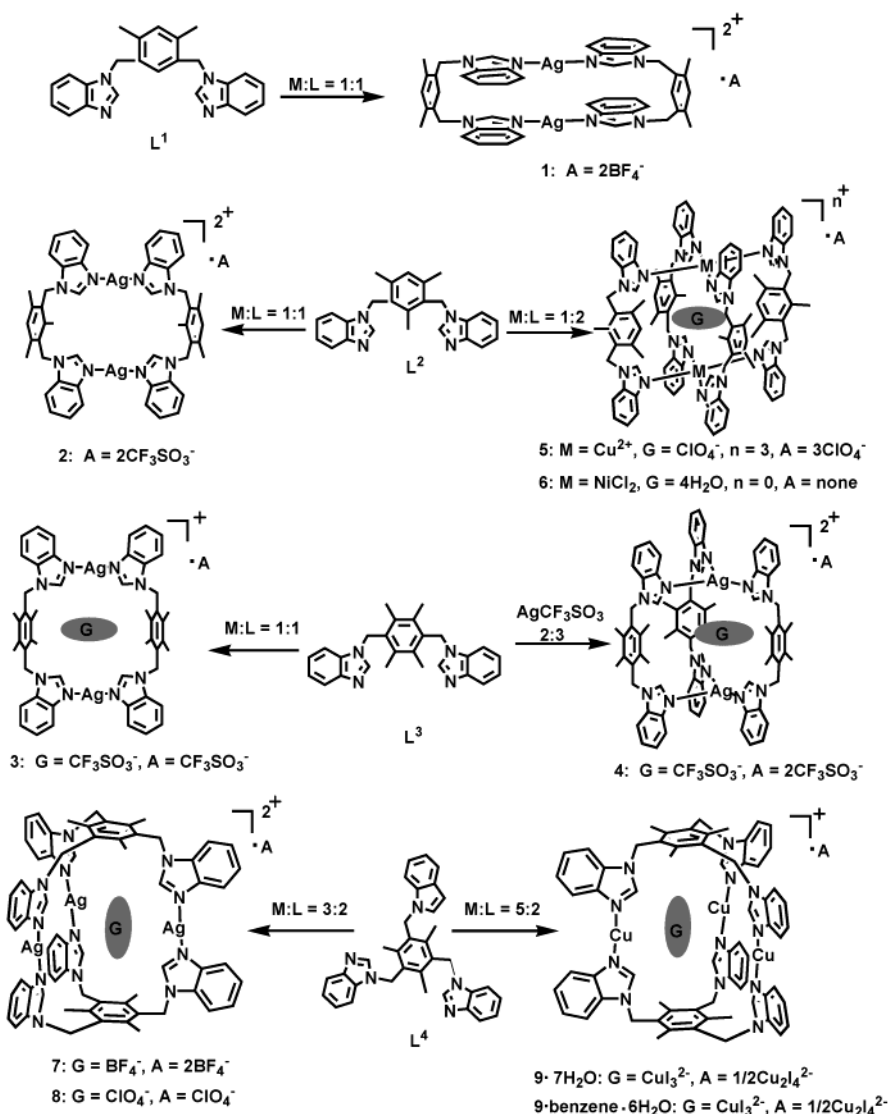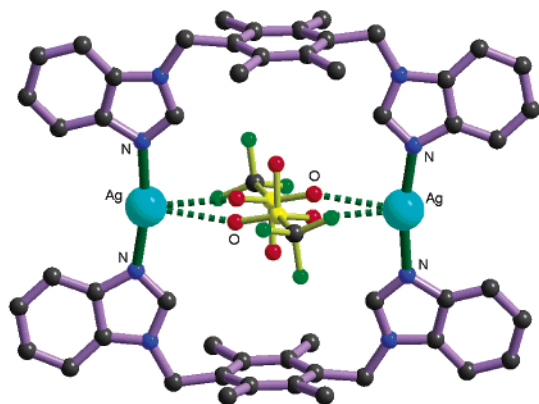
Figure 3. Ball and stick representation of the $[CF_3SO_3^- \subset Ag_2L^3{}_2]^+$ cation in **3** including the disordered $CF_3SO_3^-$ guest.

depicted in Figure 3. The Ag–N bond distances of **1**–**3** are very similar (Table S1) and consistent with those found in other two-coordinated Ag(I) complexes containing the Bim group, for example, in $[Ag_2(PyBim)_2]^{2+}$ cations (2.135–2.197 Å, **PyBim** = 2-(3-pyridyl)benzimidazole)[26] or in the [Ag$_3$-(**Etntb**)$_2$]$^{3+}$ cation (2.075–2.096 Å, **Etntb** = tris(1-ethyl-benzimidazol-2-ylmethyl)amine),[25] but somewhat shorter than those found in Ag(I) complexes with quinoline-base ligands, [Ag(**ODOQ**)]$^+$ (2.175–2.444 Å, **ODOQ** = O,O'-bis(8-quinolyl)-1,8-dioxaoctane).[27] The Ag⋯O interactions in **2** and **3** are sometimes considered to be dative bonds[7b] in which case the coordination geometry of the Ag(I) ions may be described as "T"-shaped.[7s,7t] The N–Ag–N angle is close to linearity in **1** but decreases by 7.95° and 19.79° in **3** and **2**, respectively, exhibiting different degrees of "bending".

Since Ag$^+$ is used in all three cases and since all three ligands have the same substituting arms, the overall shapes of the above structures are apparently dominated by the arene core of each ligand. L^1 and L^2 resemble each other in their *meta*-substitution patterns but differ in the substituents at the basal bridging rings: L^1 possesses a 4,6-dimethylbenzene core, while L^2 contains a 2,4,6-trimethylbenzene core. Replacement of a hydrogen atom at the 2-position by a methyl group is expected to push the two coordinating substituents away from each other. Therefore, the two Bim rings in L^1 can be oriented in a parallel fashion (dihedral angle $\tau = 19.5°$; centroid-to-centroid distance $d = 4.63$ Å) and can be folded at the methylene groups from the basal ring (C–C–N angle 113.73(2)°; $\tau = 81.5°$) in a chairlike *syn*-conformation. Two Ag$^+$ ions, related by 2-fold symmetry, connect the "chairs" to give a molecule with approximate dimensions of 18.3 Å in length and 8.9 Å in width. However, the face-to-face arrangement of the two arms positions the Ag$^+$ ions close together and reduces the resulting molecular cavity, creating an internal space of about 4.6 × 11.2 Å^2 which is defined by the separation between the two metal ions and the two basal rings (see Figure 1S; please note that these and subsequent dimensions do not take into account the van der Waals radii but are just dimensions based on the crystallographic locations of the pendent groups). In contrast, the additional methyl group in L^2 prevents a parallel alignment of the two Bim arms, which leads to a twisted head-to-head *syn*-conforma-

tion, leaving a 40.3° dihedral angle between the two arms. The basal mesitylene core is almost perpendicular to the two Bim rings (average $\tau = 91.8°$), generating a wider structure with overall dimensions of 15.1 × 11.0 Å^2 which encloses a rectangular internal cavity of ca. 6.0 × 11.0 Å^2 size (see Figure S2). The ligand L^3 has two arms in *para*-positions of a durene core so that an exact head-to-head *syn*-conformation is favored and the two Bim rings are nearly coplanar ($\tau = 11.6°$) with each other and perpendicular to the durene core (average $\tau = 89.3°$). An almost perfect rectangle of approximate size 16.9 × 10.5 Å^2 is formed, and the internal size can be estimated to be 7.8 × 10.5 Å^2 (see Figure S3). The relatively narrow cavity in **1** is presumably the reason it was found empty. The acetonitrile solvent molecules and BF$_4^-$ anions are located around the metallacycle with almost negligible Ag⋯F (3.401 Å) and Ag⋯N (3.021 Å) interactions. In **2**, two $CF_3SO_3^-$ anions are attached to the macrocycle with weak Ag⋯O interactions; they may be regarded as guest molecules. In **3**, on the other hand, one $CF_3SO_3^-$ anion is unambiguously located inside the rectangular box to give a $[CF_3SO_3^- \subset Ag_2L^3{}_2]^+$ cation, although it is crystallographically disordered.

The common feature of these three macrocycles lies in the fact that they are assembled from two ligands in a cisoid relationship and two metal ions whose potential symmetry determines the overall structures. Going from **1** to **3**, the molecules exhibit an increasingly regular shape, especially with respect to the inner rectangular cavity. This cavity, however, is arguably not a rectangular box[28] because not all the sides are truly face-to-face parallel. The term "molecular loop" has been utilized to describe similar dinuclear macrocycles,[29] and in the present cases, the structures are unique in their well-defined forms and cavity shapes generated by the tailored ligands. The construction of rectangular architectures remains a significant challenge, and molecular rectangles have remained rather uncommon,[30] compared with the multitude of molecular square analogues. Consequently, the present approach, which resembles the known strategy for assembling molecular rectangles involving cofacial chelators,[31] represents a welcome alternative method for fabricating molecular architectures with predefined rectangular cavities.

M$_2$L$_3$ or M$_3$L$_2$ Trigonal Prisms. As shown in Figure 4, the structure of **4** exhibits a canonical trigonal prismatic shape composed of two metal ions and three ligands.[16a] Each ligand

(26) Su, C.-Y.; Yang, X.-P.; Liao, S.; Mak, T. C. W.; Kang, B.-S. *Inorg. Chem. Commun.* **1999**, *2*, 383.
(27) Cai, Y.-P.; Zhang, H.-X.; Xu, A.-W.; Su, C.-Y.; Chen, C.-L.; Liu, H.-Q.; Zhang, L.; Kang, B.-S. *J. Chem. Soc., Dalton Trans.* **2001**, 2429.

(28) Dinuclear molecular rectangular boxes: (a) Kawano, T.; Kuwana, J.; Du, C. X.; Ueda, I. *Inorg. Chem.* **2002**, *41*, 4078. (b) Fujita, M.; Aoyagi, M.; Ibukuro, F.; Ogura, K.; Yamaguchi, K. *J. Am. Chem. Soc.* **1998**, *120*, 611. (c) Fujita, M.; Ibukuro, F.; Yamaguchi, K.; F.; Ogura, K. *J. Am. Chem. Soc.* **1997**, *117*, 4175. (d) Dixon, F. M.; Eisenberg, A. H.; Farrell, J. R.; Mirkin, C. A. *Inorg. Chem.* **2000**, *39*, 3432.
(29) (a) Cotton, F. A.; Chun, L.; Murillo, C. A. *Inorg. Chem.* **2001**, *40*, 472. (b) Cotton, F. A.; Chun, L.; Murillo, C. A. *Acc. Chem. Res.* **2001**, *34*, 759.
(30) For example, see: (a) Benkstein, K. D.; Hupp, J. T.; Stern, C. L. *J. Am. Chem. Soc.* **1998**, *120*, 12982. (b) Benkstein, K. D.; Hupp, J. T.; Stern, C. L. *Inorg. Chem.* **1998**, *37*, 5404. (c) Mines, G. A.; Tzeng, B.-C.; Stevenson, K. J.; Li, J.; Hupp, J. T. *Angew. Chem., Int. Ed.* **2002**, *41*, 154. (d) Woessner, S. M.; Helms, J. B.; Shen, Y.; Sullivan, B. P. *Inorg. Chem.* **1998**, *37*, 5406. (e) Rajendran, T.; Manimaran, B.; Lee, F.-Y.; Lee, G.-H.; Peng, S.-M.; Wang, C. M.; Lu, K.-L. *Inorg. Chem.* **2000**, *39*, 2016. (f) Manimaran, B.; Rajendran, T.; Lu, Y. L.; Lee, G. H.; Peng, S. M. *J. Chem. Soc., Dalton Trans.* **2001**, 515. (g) Suzuki, H.; Tajima, N.; Tatsumi, K.; Yamamoto, Y. *Chem. Commun.* **2000**, 1801. (h) Yan, H.; Süss-Fink, G.; Neels, A.; Stoeckli-Evans, H. *J. Chem. Soc., Dalton Trans.* **1997**, 4345.
(31) (a) Sommer, R. D.; Rheingold, A. L.; Goshe, A. J.; Bosnich, B. *J. Am. Chem. Soc.* **2001**, *123*, 3940. (b) Maverick, A. W.; Buckingham, S. C.; Yao, Q.; Bradbury, J. R.; Stanley, G. G. *J. Am. Chem. Soc.* **1986**, *108*, 7430. (c) Maverick, A. W.; Ivie, M. L.; Waggenspack, J. H.; Fronczek, F. R. *Inorg. Chem.* **1990**, *29*, 2403. (d) Visinescu, D.; Andruh, M.; Muller, A.; Schmidtmann, M.; Journaux, Y. *Inorg. Chem. Commun.* **2002**, *5*, 42.
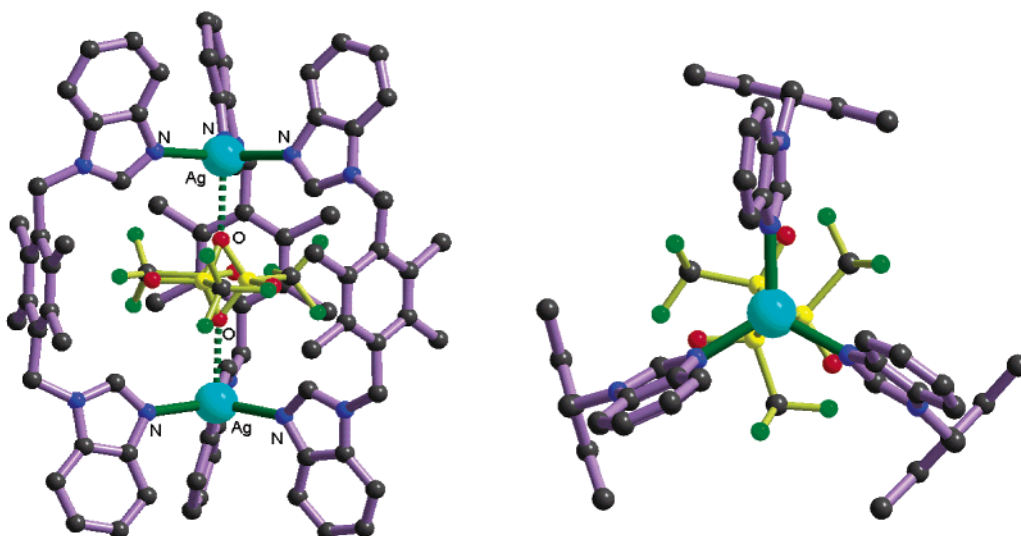
Figure 4. Ball and stick representation of the $[CF_3SO_3^- \subset Ag_2L^3_3]^+$ cation in **4**: (a) side view of the trigonal prism including a disordered $CF_3SO_3^-$ guest (left). (b) top view of the prism showing the C_3-symmetric relationship (right).

adopts the same conformation as that in **3**; however, the entire cationic prism possesses an unusual S_3 symmetry: A crystallographically imposed C_3 axis runs through two Ag(I) ions with a perpendicular mirror plane *m* across the midpoint, bisecting the trigonal prism enclosed by three 3-fold related ligands. The molecular prism hosts one triflate anion, which exhibits a crystallographically demanding a $\bar{6}$ disorder pattern with two oxygen atoms lying in the C_3 axis and weakly interacting with two Ag^+ ions (2.543(3) Å). The three Ag−N distances and N−Ag−N angles (Table S1) are symmetrically identical and the former is rather close to that in the trigonally coordinated Ag(I) network (2.261 Å) of $[Ag(TCB)(CF_3SO_3)]$,[2a] while the latter approaches the ideal value of 120° required by a triangular geometry. The overall dimensions of the prism may be estimated by an imaginary outer cylinder having a diameter of 13.6 Å and a height of 16.6 Å. The inner cavity may be described by the Ag···Ag separation of 7.5 Å and the edge lengths (9.7 Å) of the equilateral triangle defined by the centers of the three phenyl rings (see Figure S4).

Alternatively, a trigonal prismatic cage can also be obtained by utilizing the tripodal ligand **L⁴** in combination with three two-coordinated metal ions, as shown in Scheme 2. Reaction of excess $AgBF_4$, $AgClO_4$, or CuI with **L⁴** gives rise to related M_3L_2 cage structures, which are not significantly affected by the counteranions, metal-to-ligand ratio, or the solvents used. X-ray analyses show that the asymmetric unit cell of the crystal obtained from the reaction of $AgBF_4$ with **L⁴** contains one $[BF_4^- \subset Ag_3L^4_2]^{2+}$ cation, two BF_4^- anions, and one CH_3CN and one H_2O molecule,[16b] while that from the reaction of $AgClO_4$ with **L⁴** contains a cation resembling $[ClO_4^- \subset Ag_3L^4_2]^{2+}$, two ClO_4^- anions, and one CH_3CN, half of a MeOH, and a quarter of a H_2O molecule. Excess CuI reacts with two **L⁴** ligands to give a structure consisting of two independent $[CuI_3^{2-} \subset Cu_3L^4_2]^+$ cations, one $Cu_2I_4^{2-}$ anion and seven water molecules. In the presence of benzene, one water molecule can be replaced by a benzene molecule, leaving the other motifs basically intact.[16b] Figures 5 and 6 exhibit the representative cages of $[ClO_4^- \subset Ag_3L^4_2]^{2+}$ and $[CuI_3^{2-} \subset Cu_3L^4_2]^+$, in which different kinds of guest molecules are accommodated. The two silver cages are virtually identical except for the presence of different guest
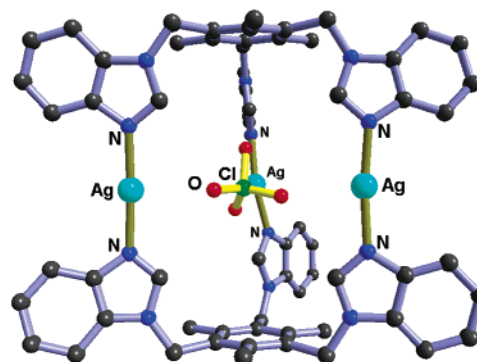

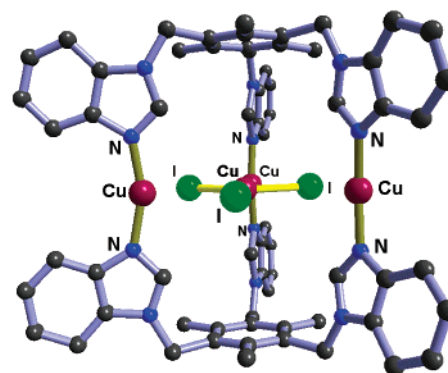**Figure 5.** Ball and stick representation of the $[ClO_4^- \subset Ag_3L^4_2]^{2+}$ cation in **8** including a ClO_4^- guest.

Figure 6. Ball and stick representation of one of the two independent $[(CuI_3)^{2-} \subset Cu_3L^4_2]^+$ cation in **9** including a $(CuI_3)^{2-}$ guest.

anions. Three almost linearly coordinated Ag^+ ions join two *syn*-conformational ligands to form a slightly distorted trigonal prism with six Bim arms nearly perpendicular to the central mesitylene cores. All the Ag−N bonds fall in the range of 2.081 to 2.117 Å (Table S1) which is similar to that of the two-coordinated Ag(I) structures **1** and **2** but a little shorter than that of **4** with three-coordinated Ag(I). In contrast, the copper-containing cages show different distortions, even for the same guest molecule and for the same asymmetric unit cell. The Cu−N bonds lengths are more varied and the N−Cu−N angles
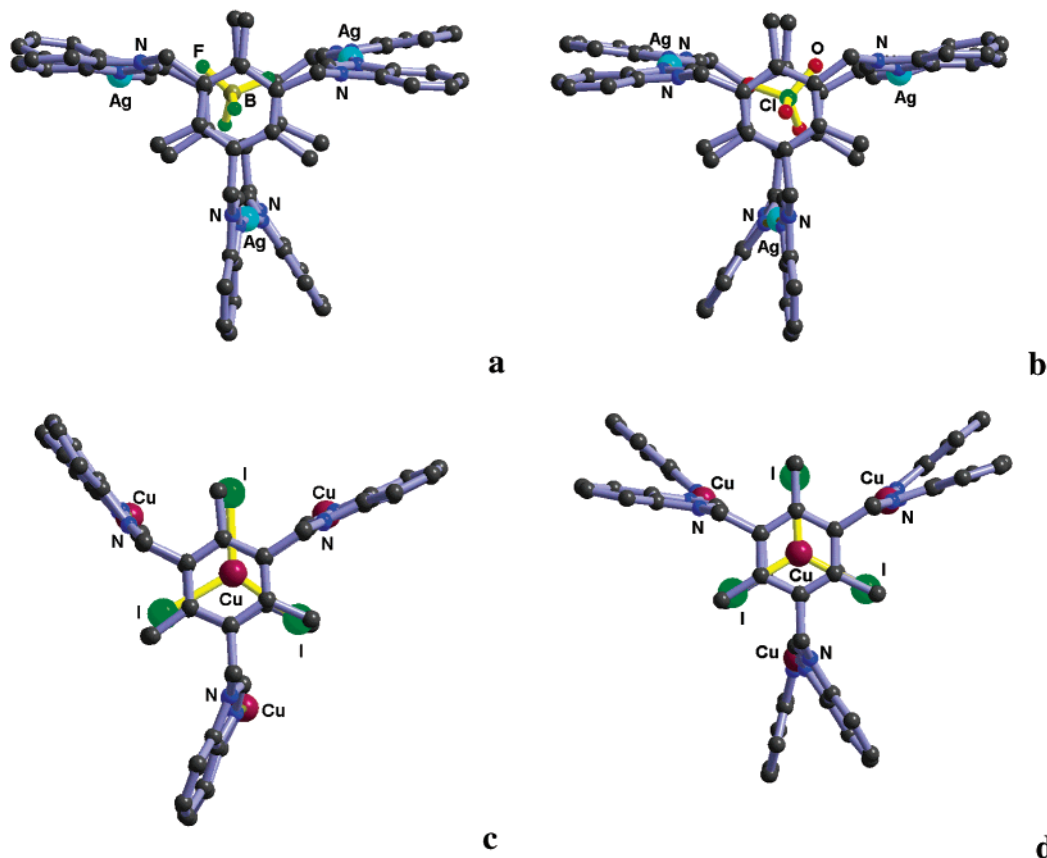
Figure 7. Perspective view of the motifs [BF$_4^-$ ⊂ Ag$_3$L$^4_2$]$^{2+}$ in **7**·CH$_3$CN·H$_2$O (a) (left top), [ClO$_4^-$ ⊂ Ag$_3$L$^4_2$]$^{2+}$ in **8**·MeCN·0.5MeOH·0.25H$_2$O (b) (right top), and [(CuI$_3$)$^{2-}$ ⊂ Cu$_3$L$^4_2$]$^+$ in **9**·7H$_2$O (c and d) (bottom).

deviate significantly from linearity when compared with N−Ag−N in the silver cages. However, both the silver and the copper cages have a common feature in that the ligands adopt the vertical *syn*-conformation. For that reason, the resulting cages exhibit a prismatic structure rather than the more common helical arrangement.[32]

Deviations from the ideal trigonal prismatic shape are easily seen in the perspective view of Figure 7. In contrast to the situation of **4**, the trigonal shapes of the structures are determined by the ligands rather than by the inherent symmetry of the metal configurations; this introduces a degree of lability to the structure because of the flexible methylene groups. As shown in Figure 7a and b, two ligands in each silver cage could be considered to form a "T" shape, which breaks the C_3 symmetry. The existence of one "slanting" leg also destroys the potential mirror plane through the three Ag$^+$ ions. Interestingly, the two silver cages in **7** and **8** form a pair of apparently enantiomeric cages, indicative of nearly identical shapes in both cases. One of the [CuI$_3^{2-}$ ⊂ Cu$_3$L$^4_2$]$^+$ cages in **9**·7H$_2$O displays a propeller shape (Figure 7c), containing a *pseudo-C$_3$* axis that passes through the central rings of two mesitylene cores and a *pseudo-σ$_h$* mirror plane involving three Cu$^+$ ions, thereby imposing a potential C_{3h} symmetry on the cage. By contrast, the second copper cage in the same unique cell is slightly irregular in that two ligands apparently show an opposite arrangement. A *pseudo-C$_2$* symmetry appears to run through each Cu$^+$ ion, thus contributing to a virtual D_3 symmetry of this cage. Similarly, the two independent copper cages in **9**·benzene·6H$_2$O also display different appearances to break any symmetric relationship

between them; however, in all cases the three iodine atoms of the triangular CuI$_3^{2-}$ guests are exactly eclipsed with the 2,4,6-positioned methyl groups, yielding virtual $σ_h$ or C_2 symmetry. It is evident that the bulky arms of such huge molecules are sensitive to the environment in the solid state. The shapes and sizes of the counteranions and solvate molecules may play an important role in the crystal packing mode, thereby influencing the crystallographic symmetry. In solution, such factors would be minimized and the symmetry of the entire molecule might be expected to be as high as D_{3h}.

The silver and copper cages possess similar overall dimensions which, as in cage **4**, may be estimated by an imaginary outer cylinder of a 16 Å diameter and 12 Å height. The internal cavity is quite regular, in contrast to the outer appearance, having an approximate size of 11 Å (height) by about 6 Å (distance between the edges, see Figure S5−7). Both the M$_2$L$_3$ and M$_3$L$_2$ metallacages are capable of encapsulating anionic guest molecules that include spherical BF$_4^-$ or ClO$_4^-$ and rodlike CF$_3$SO$_3^-$. Most interestingly, a planar CuI$_3^{2-}$ dianion (Figure 8a) is encapsulated in the copper cages, providing a unique inclusion phenomenon as we stated in the preliminary communication.[16b] Outside the cage, there are neutral molecules, such as water and benzene, and, more importantly, an interesting Cu$_2$I$_4^{2-}$ counteranion, in which two Cu$^+$ ions are symmetrically

(32) (a) Xu, J.; Parc, T. N.; Raymond, K. N. *Angew. Chem., Int. Ed.* **1999**, *38*, 2878. (b) Albrecht, M. *Chem.—Eur. J.* **2000**, *6*, 3485. (c) Yeh, R. M.; Ziegler, M.; Johnson, D. W.; Terpin, A. J.; Raymond, K. N. *Inorg. Chem.* **2001**, *40*, 2216. (d) Kim, H.-J.; Moon, D.; Lah, M. S.; Hong, J.-I. *Angew. Chem., Int. Ed.* **2002**, *41*, 3174.
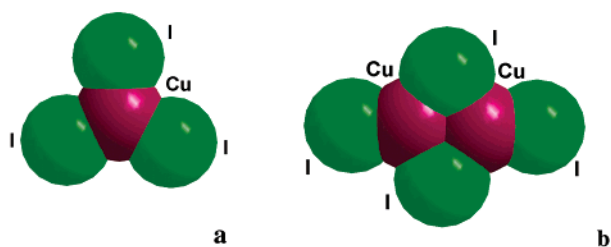
Figure 8. CPK model presentations of $(CuI_3)^{2-}$ (a) and $(Cu_2I_4)^{2-}$ anions (b) in **9**.

bridged by two out of the four I^- ligands, leading to a dimer of triangularly coordinated Cu(I), as shown in Figure 8b.

The described trigonal prismatic M_2L_3 or M_3L_2 metallacages are the smallest canonical 3D architectures with the topology based on two 3-connecting nodes joined together by three node-to-node connectors.[8a] The inherent difference between these two cage structures arises from the nature of the 3-connecting nodes, that is, whether they are formed by the metal ions (M_2L_3) or by the ligands (M_3L_2). Thus, these two cases represent two complementary strategies for generating a pair of compositionally and geometrically different but topologically identical trigonal prisms, as illustrated in Scheme 2. The former method requires a trigonal planar coordinated metal center. It is therefore surprising that Ag(I), although known to adopt trigonal geometry, for example, to generate (6,3) topological networks,[2a,7c] has appeared in only very few discrete molecular architectures assembled by utilizing this coordination mode. The most closely related example may be found in the trigonal gold(I) cage $[Au_2(\textbf{P}_2\textbf{Phen})_2]^{3+}$ ($\textbf{P}_2\textbf{Phen}$ = 2,9-bis(diphenylphosphino)-1,-10-phenanthroline)[33a] which has a D_3 symmetry and which encapsulates Tl^+ or Na^+ as cationic guests. The authors subsequently extended this system to Ag(I), Pt(0), and Pd(0) atoms, with increasingly prominent helical arrangements of the ligands.[33] In contrast, the second strategy is more widespread, as evident from the appearance of reports on M_3L_2 cages in the literature.[34] However, the majority of them deviate from the canonical trigonal prismatic structure because of the square planar or tetrahedrally coordinated metal ions used in their assembly. A very similar cage structure is that of $[Ag_3\textbf{L}_2]^{3+}$ (L = 1,3,5-tris-(imidazol-1-ylmethyl)-2,4,6-tri-methylbenzene)[34g] in which Ag^+ ions are linearly coordinated. Other molecular architectures having the trigonal prismatic structure are Rauchfuss's cyanometalate cage,[35a] Lehn's molecular cylinder,[3a,b,35b] and Fujita's interlocked supramolecule.[35c]

M_2L_4 Tetragonal Prisms. Following an approach similar to that used for the preparation of the dinuclear **2** and the trigonal prism **4**, the use of metal ions with preferred square planar
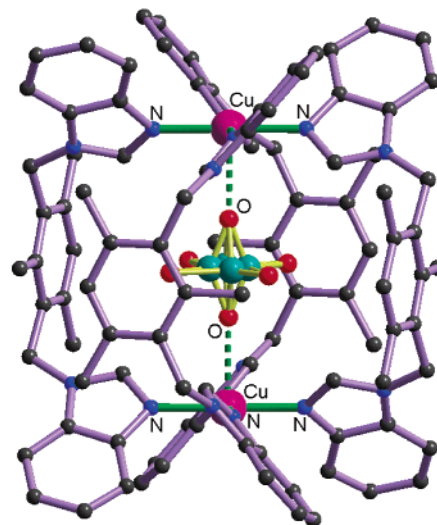
(33) (a) Catalano, V. J.; Bennett, B. L.; Kar, H. M. *J. Am. Chem. Soc.* **1999**, *121*, 10235. (b) Catalano, V. J.; Kar, H. M.; Bennett, B. L. *Inorg. Chem.* **2000**, *39*, 121. (c) Catalano, V. J.; Bennett, B. L.; Nollb, B. C. *Inorg. Chem.* **2000**, 1423.

(34) (a) Fujita, M.; Nagao, S.; Ogura, K. *J. Am. Chem. Soc.* **1995**, *117*, 1649. (b) Hiraoka, S.; Fujita, M. *J. Am. Chem. Soc.* **1999**, *121*, 10239. (c) Liu, H. K.; Sun, W. Y.; Ma, D. J.; Yu, K. B.; Tang, W. X. *Chem. Commun.* **2000**, 591. (d) Radhakrishnan, U.; Schweiger, M.; Stang, P. J. *Org. Lett.* **2001**, *3*, 3141. (e) VanCalcar, P. M.; Olmstead, M. M.; Balch, A. L. *Chem. Commun.* **1996**, 2597. (f) Ikeda, A.; Yoshimura, M.; Udzu, H.; Fukuhara, C.; Shinkai, S. *J. Am. Chem. Soc.* **1999**, *121*, 4296. (g) Sun, W.-Y.; Fan, J.; Okamura, T.; Xie, J.; Yu, K. B.; Ueyama, N. *Chem.—Eur. J.* **2001**, *7*, 2557.

(35) (a) Contakes, S. M.; Rauchfuss, T. B. *Angew. Chem., Int. Ed.* **2000**, *39*, 1984. (b) Baxter, P. N. W.; Lehn, J.-M.; Baum, G.; Fenske, D. *Chem.— Eur. J.* **1999**, *5*, 102. (c) Fujita, M.; Fujita, N.; Ogura, K.; Yamagach, K. *Nature* **1999**, *400*, 52.
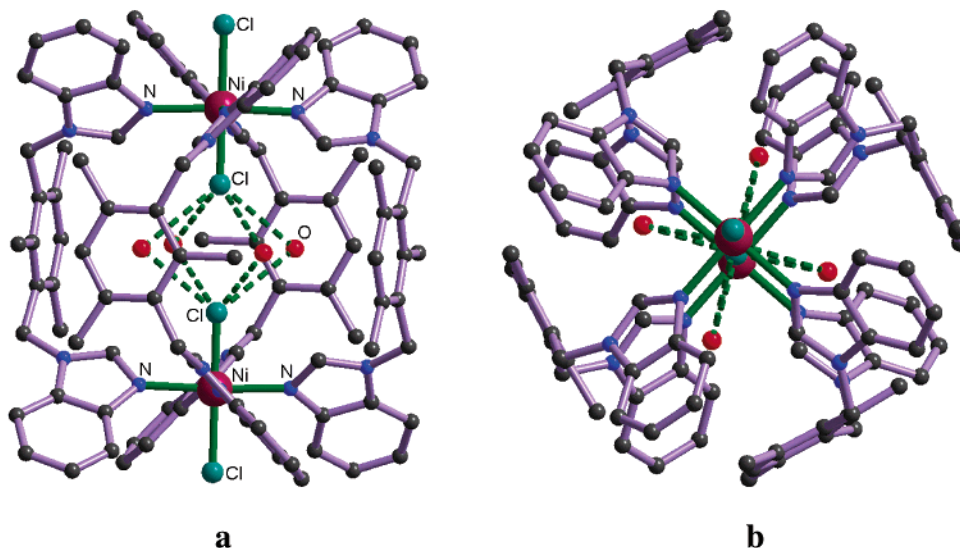

Figure 9. Ball and stick representation of the $[ClO_4^- \subset Cu_2\textbf{L}^3_4]^{3+}$ cation in **5**.

coordination geometry and four *syn*-conformational ligands leads to the formation of a tetragonal prismatic cage structure. The Cu^{2+} ion is a good candidate for square planar coordination and can thus be used in the construction of a canonical tetragonal prism $[ClO_4^- \subset Cu_2\textbf{L}^2_4]^{3+}$ (Figure 9), which was reported by us in a preliminary communication.[16a] Here, a similar tetragonal prism with nickel and no overall charge, $[4H_2O \subset Ni_2\textbf{L}^2_4Cl_2]$, is described. As shown in Figure 10a, the linear $NiCl_2$ moiety provides four open equatorial sites to bind four $\textbf{L}^2$ ligands which are attached to another $NiCl_2$, using their second binding site, to form a tetragonal prism. Thus, two Ni^{2+} ions are held by Bim arms from four C_4-symmetrically arranged ligands via four equivalent Ni−N bonds, with the octahedral coordination around the nickel being completed by the axial chloride ions. Four sides of the tetragonal prism are formed by four basal mesitylene cores, as depicted in Figure 10b, leaving four small windows in comparison with the trigonal prism **4**. As in the copper prism **5**, there is a crystallographically imposed C_4 axis passing through the two Ni^{2+} ions and a perpendicular σ_h mirror located in the center of the molecule, resulting in S_4 symmetry for the cage. The overall dimensions of the prism are approximately 11.9 × 13.5 $Å^2$, and the internal size can be defined by the nickel−nickel distance of 7.7 Å and the distance between the two parallel mesitylene rings of 10.5 Å.

The most important feature of this structure lies in the fact that the tetragonal prism itself is neutral, in contrast to the +4 charged copper analogue **5**. Instead of a charge balancing anionic perchlorate ion in **5**, four 4-fold symmetrically arranged water molecules are accommodated inside the cavity of **6**, which are well ordered and held in place by weak O−H···Cl (O···Cl, 4.555 Å) hydrogen bonds. This observation suggests that a variety of guest molecules with different properties can be selectively adsorbed into the host cage by judicious modification of the cage itself.

The high symmetry possessed by the metal ions in both the copper and nickel prisms requires that the four equatorial M−N bonds are identical and that all metal centered angles are approaching their ideal values (Table S1). The axial substituents retain the appropriate symmetry to meet the topological requirements of the tetragonal prism: two 4-connecting nodes linked together by four node-to-node connections.[8a] Similar to the

Figure 10. Ball and stick representation of the [$4H_2O \subset Ni_2L^3_4$] cage in **6**: (a) side view of the tetragonal prism including four guest water molecules and (b) top view of the prism showing the C_4-symmetric relationship.
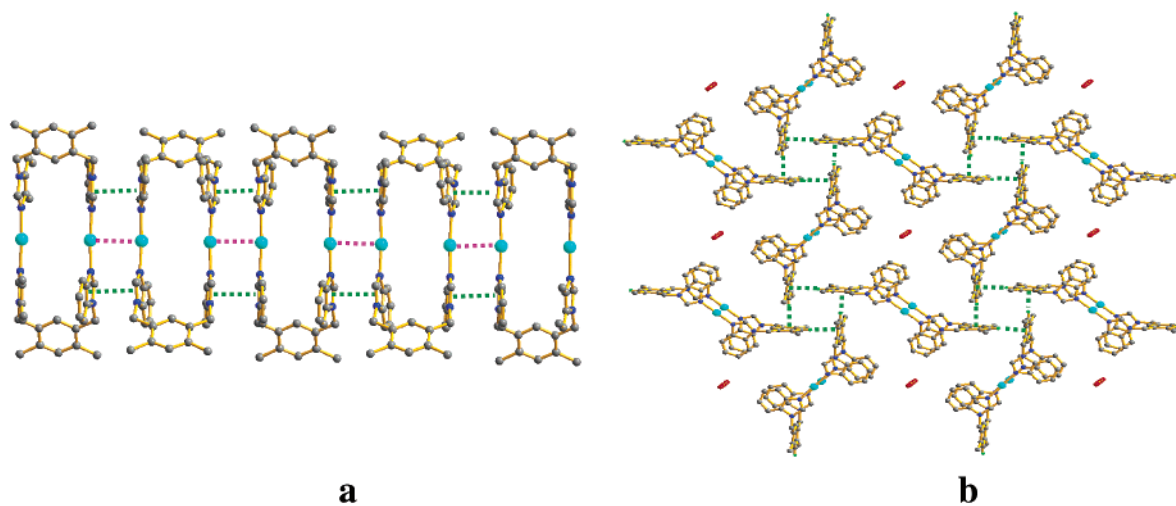

Figure 11. (a) Parallel arrangements of the metallacycles in **1** linked by weak Ag···Ag and π···π interactions. (b) C−H···π interactions at the *ab* plane and channels along the *c* direction. The guest acetonitrile molecules are marked in red. The $CF_3SO_3^-$ anions are omitted for clarity.

above-mentioned M_2L_3 and M_3L_2 topological pairs, the M_4L_2 counterpart of the present M_2L_4 cage can be envisioned by connecting a four-branched *syn*-conformational ligand such as 1,2,4,5-tetrakis(benzimidazol-1-ylmethyl)benzene (**L^5**) with four linearly coordinated metal centers. Unfortunately, the rather low solubility prevents **L^5** from being effectively used in any solid-state or solution investigation. One relevant example comes from Dalcanale's D_{4h} symmetrical M_4L_2 cage, which forms in solution from the interaction of two preformed cavitands with four square planar metal bis-triflates.[36a] Several M_2L_4 cage structures[36b−e] have appeared in the literature in which the metal atoms typically display a square geometry or require further axial interaction, allowing for easy modification. A more extensive study may have to be undertaken to explore this issue since, although a structurally similar [$Pd_2(S_7)_4$]$^{4-}$ cage was reported in 1986,[36f] both cases remain quite rare.

Crystal Packing. In the fast developing field of crystal engineering and coordination polymers, special attention is paid to the pores that are often created in such framework materials. In contrast, the voids formed outside and between discrete molecular architectures have sometimes been overlooked. These

voids, like potential pores or channels, can easily form between such molecular species, and it is possible to think of large molecules as the building blocks for multidimensional network structures.[2c,14e,37] The ability of gas storage or guest transport by such structures has been well demonstrated.[38] In **1**, the intermolecular weak Ag···Ag interactions (3.414 Å) and π···π contacts formed between parallel Bim rings ($d = 3.364(2)$ Å; $\tau = 3.80°$) connect the [$Ag_2L^1_2$]$^{2+}$ metallacycles into a chain, as shown in Figure 11a. Such chains are aligned side-by-side in the *c* direction, where one of the two benzene cores of each metallacycle is oriented in a head-on fashion with the benzene

(36) (a) Jacopozzi, P.; Dalcanale, E. *Angew. Chem., Int. Ed. Engl.* **1997**, *36*, 613. (b) Chand, D. K.; Biradha, K.; Fujita, M. *Chem. Commun.* **2001**, 1652. (c) Barbour, L. J.; William Orr, G.; Atwood, J. L. *Nature* **1998**, *393*, 671. (d) Owens, T. D.; Hollander, F. J.; Oliver, A. G.; Ellman, J. A. *J. Am. Chem. Soc.* **2001**, *123*, 1539. (e) McMorran, D. A.; Steel, P. J. *Angew. Chem., Int. Ed.* **1998**, *37*, 3295. (f) Müller, A.; Schmitz, K.; Krickemeyer, E.; Penk, M.; Bögge, H. *Angew. Chem., Int. Ed. Engl.* **1986**, *25*, 453.
(37) Chui, S. S.-Y.; Lo, S. M.-F.; Charmant, J. P. H.; Orpen, A. G.; Williams, I. D. *Science* **1999**, *283*, 1148.
(38) (a) Atwood, J. L.; Barbour, L. J.; Jerga, A.; Schottel, B. L. *Science* **2002**, *298*, 1000. (b) Li, H.; Eddaoudi, M.; O'Keefe, M.; Yaghi, O. M. *Nature* **1999**, *402*, 276. (c) Noro, S.-i.; Kitagawa, S.; Kondo, K.; Seki, K. *Angew. Chem., Int. Ed.* **2000**, *39*, 2082.
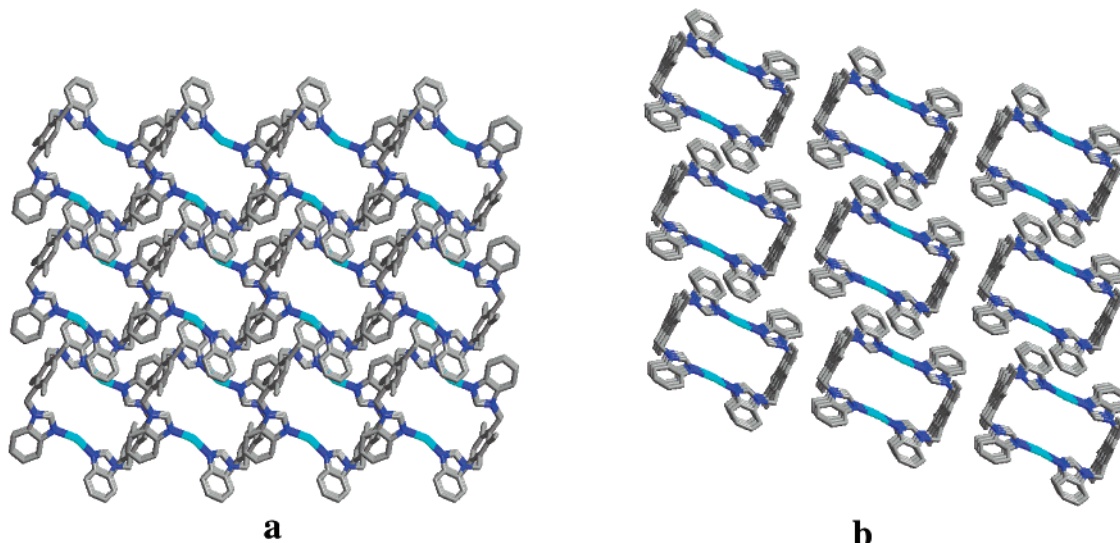
Figure 12. Square channels extended along the *c* direction in **2** (a) and slightly deflecting the *a* direction in **3** (b).
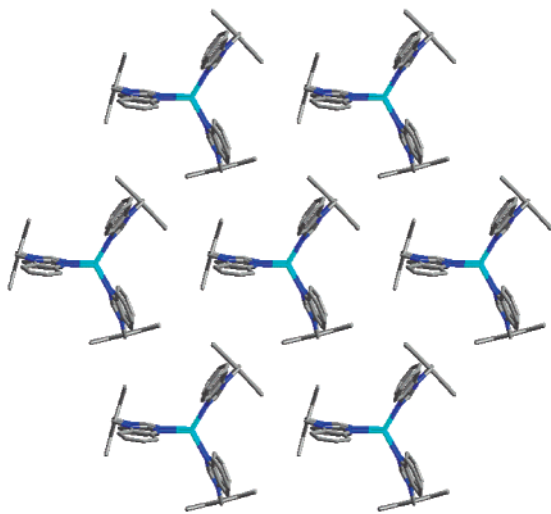

Figure 13. Three-fold arrangement of trigonal prisms in **4**.

ring of an adjacent chain. Thus, four C−H···π interactions are formed between every four neighboring chains in the *ab* plane (H···π, 2.919 Å; C−H···π, 176.95°), and the resulting 3D network contains hydrophobic channels, formed by benzene rings, as shown in Figure 11b; these channels contain disordered acetonitrile guest molecules.

In **2**, the $[Ag_2L^2_2]^{2+}$ units are arranged such that differently sized channels originating from inner cavities can be observed in all directions (see Figure 12a and S10). The $CF_3SO_3^-$ anions are located along the *c* axis. By contrast, the metallacycles of **3** are stacked one above another with four nearly coplanar Bim rings (Figure S11), leading to the rectangular channels that are occupied by $CF_3SO_3^-$ anions, as depicted in Figure 12b. A quite different arrangement is found for **4**, where the trigonal prisms are 3-fold symmetrically arranged in the *ab* plane, forming a close-packed hexagonal arrangement. (Figure 13). Such layers stack in an AB fashion, thereby excluding any possible channels. It is interesting that while the two tetragonal prisms **5** and **6** have exactly the same crystallographic symmetry, the molecular arrangement in the crystal lattice is noticeably different. In **5**, two 4-fold axially disordered ClO_4^- anions are alternately

arranged inside and outside the charged molecular cage along the C_4 axis, thereby linking the molecules into a one-dimensional column with axial Cu···O interactions (2.388 and 2.659 Å), producing polycages, as shown in Figure 14a. The entire crystal is built-up by such columns that stack side-by-side to generate open, rectangular channels occupied by perchlorate anions (Figure 14b). In neutral **6**, by comparison, the absence of bulky guest species permits the molecules to be in closer proximity, forming π···π interactions between each prism and eight neighboring units (*d* = 4.351(4) Å; τ = 0.03°). The distance between these parallel rings is 3.414 Å, which generates a 3D network sustained by π···π contacts (Figure 14c). As mentioned earlier, the crystal packing of the M_3L_2 cages is strongly influenced by the presence of counteranions and solvent molecules.

The two silver cages **7** and **8** show similar packing motifs, which may be due to the presence of similar spherical counteranions. As shown in Figure 15a, the cages are arranged in pairs and stack one above the other, giving the ligand a "T" shape conformation. No useful channels are created because of the close proximity of the Bim rings; however, there is sufficient space between linearly stacked cages to accommodate anions and solvent molecules. In contrast, the copper cages in $\mathbf{9} \cdot 7H_2O$ and $\mathbf{9} \cdot C_6H_6 \cdot 6H_2O$ show a noticeably different packing arrangement. Two independent cages in the complex are positioned in different directions related by a 90° rotation, as shown in Figure 15b. Each orientation of the cage forms one layer that alternates with another containing the cage in the second orientation, producing an extended layered structure. All guest molecules are found between cages of only one orientation, which generates the channels shown in Figure 15c and d. On the other hand, the respective orientations of individual cages in two neighboring layers are different in these two different solvate compounds which may be caused by the replacement of a water molecule in $\mathbf{9} \cdot 7H_2O$ by a benzene molecule in $\mathbf{9} \cdot benzene \cdot 6H_2O$.

Solution Structures and Dynamics. One common feature of all structures mentioned is that the ligands adopt the *syn*-conformation. However, since the ligands are only semirigid, they can in principle change to the *anti*-conformation[18] to generate polymers. The question then concerns the factors that
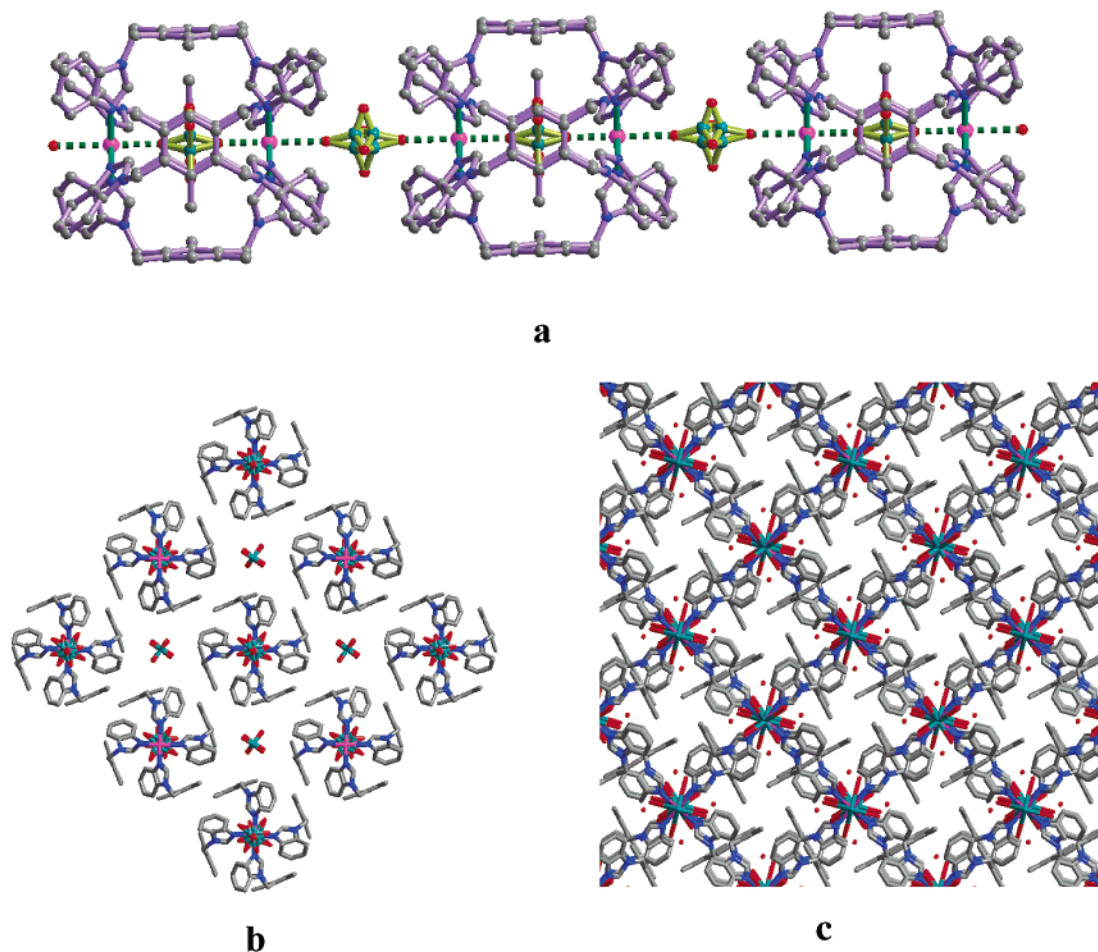
Figure 14. (a) One-dimensional polycages connected by Cu⋯O interactions in **5** (top). (b) Channels formed by parallel alignment of tetragonal prisms in **5** (left bottom). (c) 3D network formed by close packing of tetragonal prisms in **6** (right bottom).

favor the formation of closed molecular architectures with defined shapes and sizes over possible oligomers or multidimensional polymeric structures. To address this question, NMR and ESI-MS have been utilized to study the solution behavior of these assemblies. In this context, it must be mentioned that silver(I) complexes are normally labile and rapid exchange may occur on the NMR time scale at room temperature.[7r,12c] This lability, while necessary to allow for the facile self-correction during the self-assembly process, makes it more challenging to reach conclusions based solely on the NMR study. However, some informative investigations on the solution structure and dynamics of silver(I) complexes have indeed been carried out[12c,13b] and, especially when coupled with ESI-MS spectroscopy, have been very helpful for the characterization of polynuclear metal complexes.[4c,21a,39]

^{1}H NMR spectra of the ligands and of the silver(I) complexes were recorded at room temperature. In general, the spectra show a simple pattern containing one set of signals, suggesting the formation of one single species in solution or the presence of a rapid equilibrium established on the NMR time scale. The latter is certainly possible because labile Ag^{+} ions are involved in the coordination process. Compared with the spectrum of the "free" ligands, the proton signals of the complexes are shifted (downfield or upfield) and slightly broadened, clearly indicative of metal complexation in solution. Despite the possible existence of rapid chemical exchange between potential coordination

motifs, a comparison of the chemical shifts of different protons may still lead to the recognition of a dominant coordination mode in solution, especially with the support of the solid-state structural pattern.

^{1}H NMR spectra of the ligand **L[1]** and its complex **1** are depicted in Figure 16. The protons H2, H8, and H11 are shifted slightly downfield, while H4−H7 remain almost unchanged. The most remarkable change is found for H14 which is shifted upfield by 0.554 ppm. It is normal that the chemical shifts of the ligand protons experience a downfield shift due to the loss in electron density upon coordination,[10,17] and in the present case, the largest shift is expected for H2 because of its proximity to the nitrogen donor sites. However, the abnormally small shift of H2 ($\Delta\delta$ 0.221 ppm) and the tiny upfield shifts of H4−H7 ($\Delta\delta$ −0.020 to −0.043 ppm) observed for **1** are significant in that they indicate that the major species in solution retains the same structure as that found in the solid state. This suggests that the two Bim rings keep the face-to-face arrangement to shift proton signals upfield due to the ring current effect.[40] Additional evidence comes from the noticeable shift of H14. As we can see from the solid-state structure, the chairlike *syn-*

(39) (a) Hopfgartner, G.; Piguet, C.; Henion, J. D. *J. Am. Soc. Mass Spectrom.* **1994**, *6*, 748. (b) Bitsch, F.; Dietrich-Buchecker, C. O.; Khémiss, A.-K.; Sauvage, J.-P.; Dorsselaer, A. V. *J. Am. Chem. Soc.* **1991**, *113*, 4023. (c) Moucheron, C.; Mesmaeker, A. K.-D. *J. Am. Chem. Soc.* **1996**, *118*, 12834.
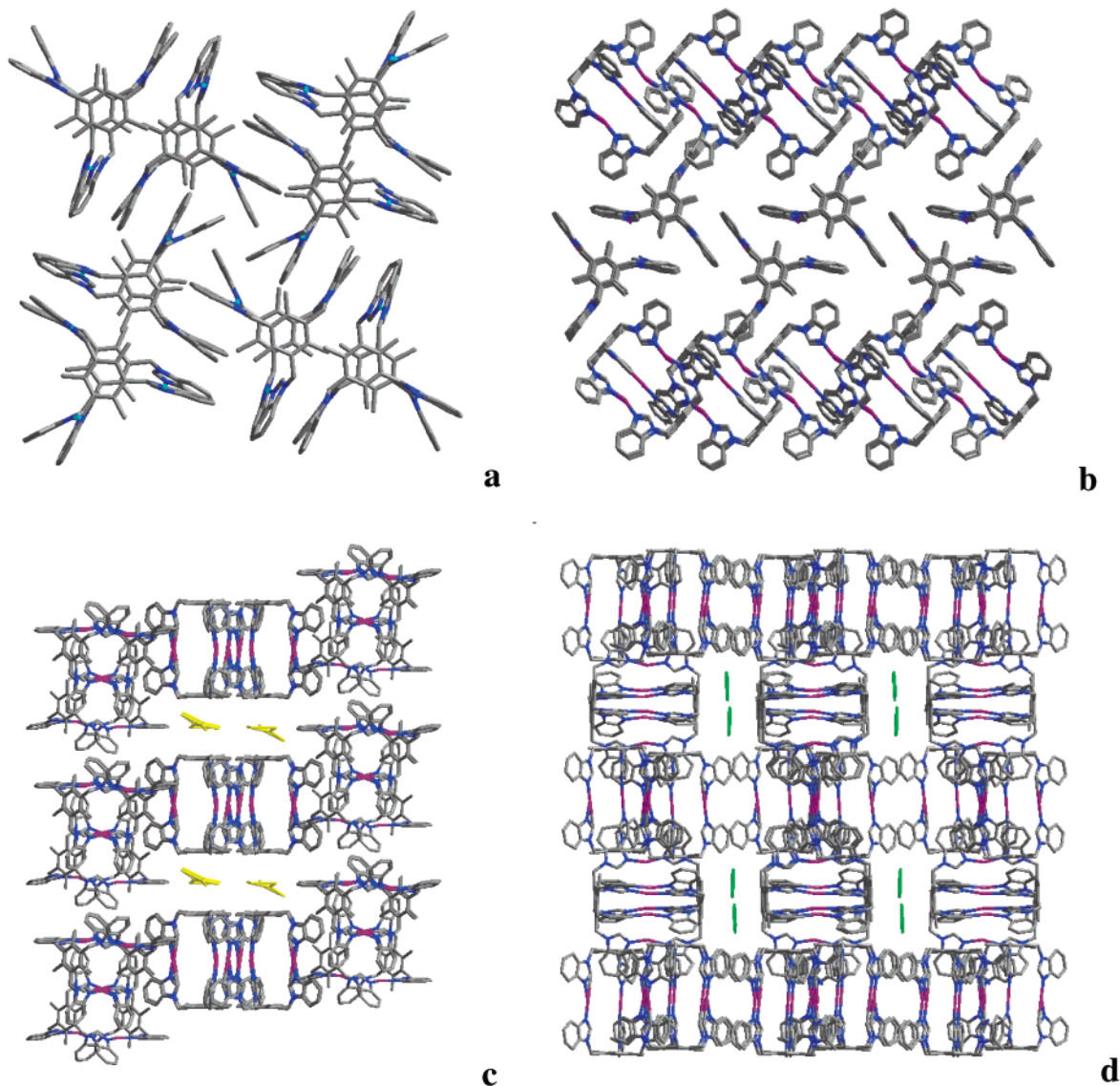
Figure 15. (a) Close packing mode in **7** and **8** in the *ab* plane composed of exactly one linear stack of metallacages along the *c* axis (left top). (b) Alternate layers formed by differently orientating metallacages in **9**·7H$_2$O (right top). (c) Channels running in the *a* direction accommodating guest molecules (yellow) in **9**·7H$_2$O (left bottom). (d) Section view at the [101] plane showing channels occupied by guest molecules (green) **9**·benzene·6H$_2$O (right bottom).
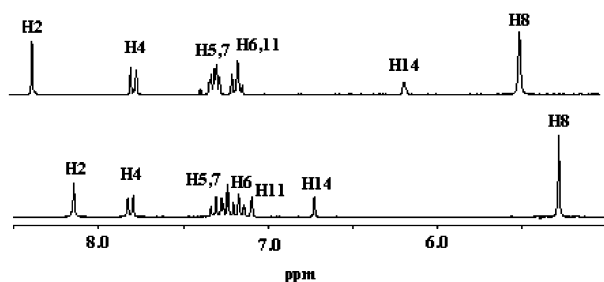

Figure 16. Partial ^{1}H NMR spectra of **L^1** (bottom) and **1** (top). The atomic numbering scheme for protons is the same as that for the carbon atoms in Scheme 1.

conformation of the ligand allows H14 to point between two face-to-face positioned Bim rings, providing a good diagnostic proton signal for the investigation of its solution structure.

(40) (a) Shetty, A. S.; Zhang, J.; Moore, J. S. *J. Am. Chem. Soc.* **1996**, *118*, 1019. (b) Mizutani, M.; Kubo, I.; Jitsukawa, K.; Masuda, H.; Einaga, H. *Inorg. Chem.* **1999**, *38*, 420. (c) Fischer, B. E.; Sigel, H. *J. Am. Chem. Soc.* **1980**, *102*, 2998. (d) Yamauchi, O.; Odani, A. *J. Am. Chem. Soc.* **1985**, *107*, 5938.

By contrast, in complexes **2**−**4** the signals of the Bim protons H4−H7 show a significant downfield shift when compared with those of the corresponding free ligand. However, a detailed study suggests that the solution structure may still be reflected by the relative chemical shifts between different protons on the same ligand. As discussed above, H2 is expected to show the largest shift in comparison with other protons; however, the vertical head-to-head *syn*-conformation of the ligand will leave H2 shielded by the ring current from the arene core. Therefore, the relatively smaller $\Delta\delta$ values of H2 in **2**−**4** agree with the formation of rectangular or prismatic structures in solution, similar to what is observed in the solid state. Similar phenomena occur for the silver and copper cages **7**−**9**. The largest $\Delta\delta$ values are found for H4 rather than for H2, suggesting that the cage structures are retained.[16b]

Support for the solution structures was convincingly provided by ESI-MS spectroscopy which was demonstrated to be able to provide an "image" of the composition of a solution.[4c] Although the experimental conditions may affect the results, the

Table 2. ESI-MS Data[a]

compound	characteristic ions
1[b]	$[AgL^1]^+$ 474.0 (474.1); $[Ag_2L^1_2(BF_4)]^+$ 1034.9 (1035.2)
2[b]	$[AgL^2]^+$ 487.0 (487.1); $[Ag_2L^2_2(CF_3SO_3)]^+$ 1124.8 (1125.2)
3[b]	$[AgL^3]^+$ 501.4 (501.1); $[Ag_2L^3_2]^{2+}$ 501.9 (502.1); $[Ag_2L^3_2(CF_3SO_3)]^+$ 1153.1 (1153.2)
4[c]	$[Ag_2L^3_2]^{2+}$ 501.9 (502.1); $[Ag_2L^3_3]^{2+}$ 699.0 (699.2); $[AgL^3_2]^+$ 897.1 (897.3);
	$[Ag_2L^3_2(CF_3SO_3)]^+$ 1152.7 (1153.2); $[Ag_2L^3_3(CF_3SO_3)]^+$ 1546.8 (1547.4)
5[d]	$[Cu_2L^2_4(ClO_4)]^{3+}$ 582.5 (582.5); $[Cu_2L^2_4(ClO_4)_2]^{2+}$ 923.2 (923.3);
	$[Cu_2L^2_4(ClO_4)_3]^+$ 1947.4 (1947.5)
6[d]	$[NiL^2_2Cl]^+$ 852.9 (853.3); $[NiL^2_3Cl]^+$ 1235.1 (1235.5); $[Ni_2L^2_3Cl_3]^+$ 1363.0 (1363.4);
	$[NiL^2_4Cl]^+$ 1615.2 (1615.7); $[Ni_2L^2_4Cl_3]^+$ 1744.9 (1745.6)
7[b]	$[AgL^4]^+$ 619.2 (619.2); $[(Ag_3L^4_2)(BF_4)]^{2+}$ 716.1 (716.1); $[(Ag_3L^4_2)(BF_4)_2]^+$ 1519.1 (519.2)
8[b]	$[AgL^4]^+$ 619.2 (619.2); $[(Ag_3L^4_2)(ClO_4)]^{2+}$ 722.2 (722.1); $[(Ag_3L^4_2)(ClO_4)_2]^+$ 1543.2 (1543.1);
	$[(Ag_4L^4_2)(ClO_4)_3]^+$ 1750.9 (1751.0)
9[e]	$[(Cu_3L^4_2)I]^{2+}$ 669.0 (669.1); $[(Cu_3L^4_2)(CuI_3)]^+$ 1654.4 (1654.9)

[a] m/z values are given for the highest isotope line in Da, and theoretical values, in parentheses. [b] In MeOH−CH$_3$CN (v/v = 1:1). [c] In DMSO. [d] In MeOH. [e] In CH$_3$CN−DMF (v/v = 2:1).
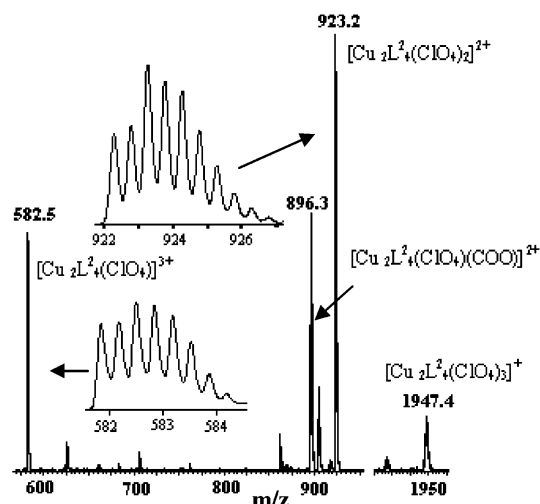

Figure 17. Partial ESI-MS spectrum of **5**. Isotopic distributions of the triple-charged $[Cu_2L^2_4(ClO_4)]^{3+}$ and double-charged $[Cu_2L^2_4(ClO_4)_2]^{2+}$ cations are amplified.

overall nature and, to some extent, the distribution of the different coordination species can be obtained. The ESI-MS spectral data are given in Table 2, where the main ions characteristic of the complexes present in solution are listed. Every ion is verified by careful comparison of the isotopic patterns between the observed peak and the theoretical simulation, confirming the consistency of the molecular mass and the stoichiometric formulation. The ESI-MS spectra of **1** and **2** display major peaks corresponding to $[(Ag_2L^1_2)(BF_4)]^+$ and $[(Ag_2L^2_2)$-$(CF_3SO_3)]^+$, respectively, evidently indicating the formation of dinuclear metallocyclic structures in solution. Peaks corresponding to the monomeric $[AgL^1]^+$ or $[AgL^2]^+$ are found, suggesting the presence of the precursors for assembly of the dinuclear target molecules.

The spectrum of **5** is dominated by peaks corresponding to the successive loss of counteranions, $[(Cu_2L^2_4)(ClO_4)_n]^{(4-n)+}$ (n = 1−3), suggesting the quantitative assembly of the tetragonal prism in the solution. The different charge states are well established by evaluation of the separations between the clearly resolved isotopic peaks as depicted in Figure 17. In addition, some species contaminated by formic acid, for instance, $[(Cu_2L^2_4)(ClO_4)(COO)]^{2+}$ (m/z 896.3), are also detectable. By contrast, **6** displays a series of signals related to different degrees of dissociation of the ligand and of the Cl$^-$ anions from the neutral cage structure. The intensity of the peaks becomes very
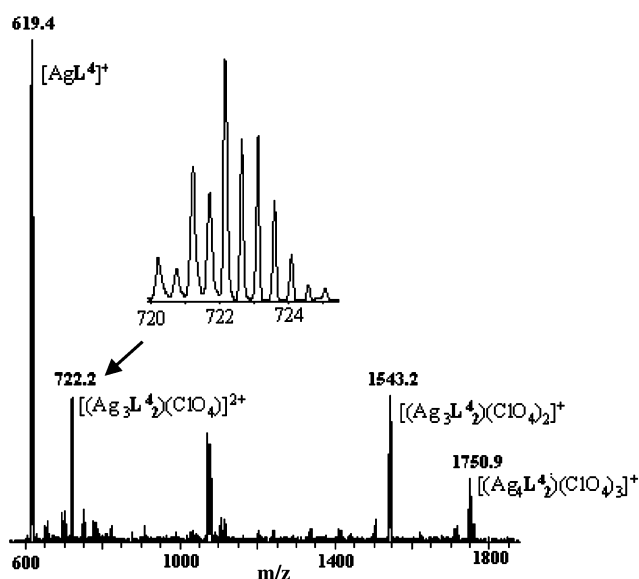

Figure 18. Partial ESI-MS spectrum of **8**. Isotopic distribution of the double-charged $[Ag_3L^4_2(ClO_4)]^{2+}$ cation is amplified.

weak, probably due to the difficulty in releasing the Cl$^-$ counteranions. The presence of the tetragonal prism is manifested by the ion $[(Ni_2L^2_4)Cl_3]^+$, which loses one ligand to give rise to $[(Ni_2L^2_2)Cl_3]^+$. Mononuclear units are detected with the Ni^{2+} ion binding to different numbers of the ligands, as demonstrated by the species $[(NiL^2_n)Cl]^+$ (n = 1−4).

The formation of the trigonal cage structure in solution coincides with the appearance of peaks corresponding to $[(Ag_3L^4_2)(BF_4)]^{2+}$ and $[(Ag_3L^4_2)(BF_4)_2]^+$ in the ESI-MS spectrum of **7**, together with some unidentified smaller peaks. In contrast, the spectrum of the analogous **8** shows a relatively clear pattern, exhibiting two expected cage species, $[(Ag_3L^4_2)$-$(ClO_4)]^{2+}$ and $[(Ag_3L^4_2)(ClO_4)_2]^+$, and three more peaks of which two are believed to be due to mononuclear $[AgL^4]^{2+}$ and tetranuclear $[(Ag_4L^4_2)(ClO_4)_3]^+$, respectively, as shown in Figure 18. The spectrum of **9** is interesting because it is simple yet informative. The major peak indicates unambiguously an $[(Cu_3L^4_2)(CuI_3)]^+$ ion, which is known from the solid-state structure to be an M$_3$L$_2$ cage containing a CuI$_3{}^{2-}$ guest molecule. On the other hand, a minor peak corresponding to $[(Cu_3L^4_2)I]^+$ was found as well. It strongly suggests a similar cage structure but one that accommodates an I$^-$ guest instead of a CuI$_3{}^{2-}$ guest. This is important because one might otherwise assume, based
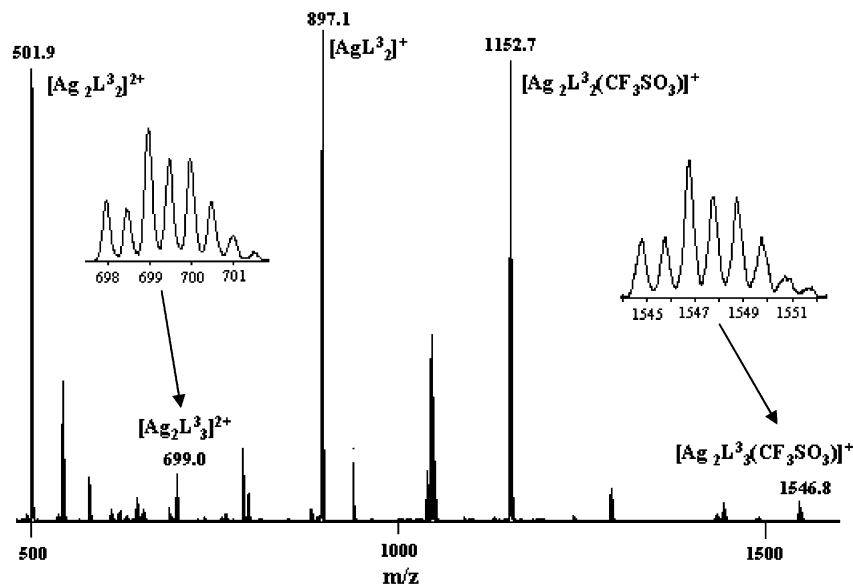
Figure 19. Partial ESI-MS spectrum of **4**. Isotopic distributions of the double-charged [Ag$_2$**L**$^3_3$]$^{2+}$ and single-charged [Ag$_2$**L**$^3_3$(CF$_3$SO$_3$)]$^+$ cations are amplified.

on the solid-state structural analyses, that the copper cage can only be formed with the aid of a CuI$_3^{2-}$ guest molecule.

The ESI-MS investigation of **3** and **4** is particularly interesting because they contain the same ligand and metal ions, although in different proportions, and have different molecular topologies. An understanding of their solution distribution is helpful for controlling the synthesis conditions to obtain one specific product. A series of spectra have been recorded in different solvent media and different metal-to-ligand ratios without separating the solid product. In an MeOH−CH$_3$CN mixture (v/v = 1:1) the spectrum obtained with a 1:1 metal-to-ligand ratio shows a major peak of the dinuclear [(Ag$_2$**L**$^3_2$)(CF$_3$SO$_3$)]$^+$ cation, accompanied by a minor peak of mononuclear [Ag**L**^{3}]$^+$. Increasing the ligand-to-metal ratio to 3:2 only results in the appearance of a little [(Ag$_2$**L**$^3_2$)]$^{2+}$ overlapping with [Ag**L**^{3}]$^+$. These two species bear the same *m/z* values (502) but can be well distinguished from one another by their completely different isotopic patterns. No peak related to M$_2$L$_3$ topology can be unequivocally assigned. In DMSO solution, on the other hand, two relatively weak peaks from [(Ag$_2$**L**$^3_3$)]$^{2+}$ and [(Ag$_2$**L**$^3_3$)-(CF$_3$SO$_3$)]$^+$, corresponding to the M$_2$L$_3$ topology, are detected, as shown in Figure 19. Addition of a small excess of ligand increases these two peaks slightly but also results in the observation of an [(Ag**L**$^3_2$)]$^+$species next to the intense peak of [(Ag$_2$**L**$^3_2$)(CF$_3$SO$_3$)]$^+$. The peak at about *m/z* = 502, however, is primarily due to the [(Ag$_2$**L**$^3_2$)]$^{2+}$ dication. These findings suggest that the distribution of the different topological species is solvent dependent. Similar observations have been reported previously by Lehn[12a,41a] and Stang[41b] and most likely are due to the different solubilities in different solvents. The relatively weak peaks observed for the M$_2$L$_3$ structure may reflect that these species are unstable under the measurement conditions. On the other hand, the coexistence of M$_2$L$_2$ and M$_2$L$_3$ topological species, together with the [(Ag**L**$^3_2$)]$^+$ motif and some other unidentified peaks, indicates that a dynamic equilibrium exists that involves a series of solution species. In another word, a
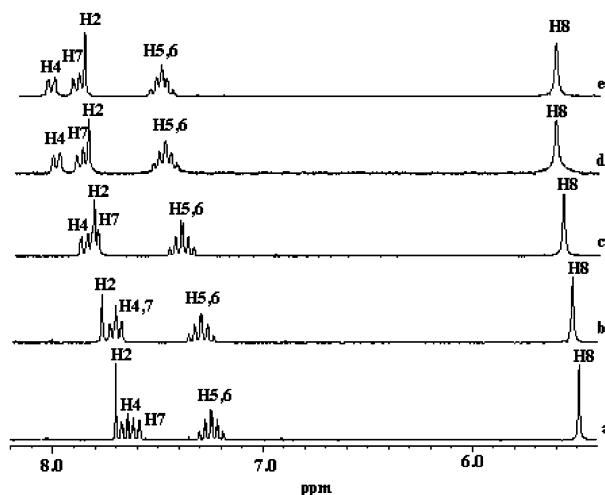
(41) (a) Baxter, P. N. W.; Lehm, J.-M.; Rissanen, K. *Chem. Commun.* **1997**, 1323. (b) Schweiger, M.; Seidel, S. R.; Arif, A. M.; Stang, P. J. *Inorg. Chem.* **2002**, *41*, 2556.

Figure 20. Monitoring of the titration of **L**^{3} with AgCF$_3$SO$_3$. Metal-to-ligand ratios: (a) pure **L**^{3}, (b) 2:4, (c) 2:3, (d) 2:2, and (e) 2:1. The atomic numbering scheme for protons is the same as that for the carbon atoms in Scheme 1.

"virtual combinatorial library"[41a,42] was established. A similar phenomenon is found for other complexes, although most of the individual members may be present only in minuscule proportions and may not be detectable by ESI-MS. Therefore, thermodynamic factors play an important role in the assembly of the present molecular architectures. To obtain further insight, the solution dynamics were investigated by means of ^{1}H NMR based on the chemical exchange allowed by the kinetically labile dative bonds.

Figure 20 depicts the *in situ* spectral monitoring of the reactions between **L**^{3} and AgCF$_3$SO$_3$ carried out in DMSO-*d*$_6$ without isolating the complexes. When the metal salt was added in a smaller amount than that required for a 2:3 stoichiometry to form the M$_2$L$_3$ complex, all protons exhibit a slight downfield shift but no signals due to the "free" ligand appear, indicating complexation and rapid chemical exchange between the Ag$^+$

(42) (a) Huc, I.; Lehn, M.-J. *Proc. Natl. Acad. Sci. U.S.A.* **1997**, *94*, 2106. (b) Lehn, J.-M.; Eliseev, A. V. *Science* **2001**, *291*, 2331.
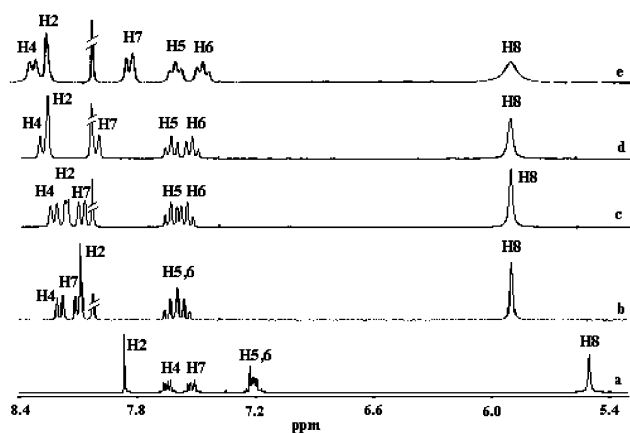
Figure 21. Temperature dependent ^{1}H NMR spectra of **7** in DMF-d_7. (a) **L^4** in DMSO-d_6, (b) 293 K, (c) 273 K, (d) 253 K, and (e) 223 K. The atomic numbering scheme for protons is the same as that for the carbon atoms in Scheme 1.

ions and excess ligand. Increasing the metal-to-ligand ratio causes a continuous downfield shift until the maximum shift was achieved at a 1:1 ratio. Further addition of AgCF$_3$SO$_3$ shows little influence on the resulting proton spectrum which is almost identical to that of the isolated M$_2$L$_2$ complex, indicative of the nearly quantitative assembly of metallacyclic **3**. In contrast, titration of AgCF$_3$SO$_3$ with the ligand only leads to the *reverse* shift of the signals (upfield), and the M$_2$L$_3$ cage structure can be expected to dominate at a metal-to-ligand ratio of 2:3 or with a small excess of the ligand. These experiments suggest that the reactions are thermodynamically controlled and that the equilibria are rapidly achieved on the NMR time scale, closely resembling the solution dynamics exhibited by the M$_3$L$_2$ silver cage structure as we reported in our preliminary communication and, therefore, will not be discussed here.[16b] On the other hand, the chemical exchange may be slowed by lowering the temperature. Figure 21 shows the temperature dependent ^{1}H NMR spectra of **7** in DMF-d_7 measured from 293 to 223 K. It is clear that the resonance signals are broadened but better separated from each other on decreasing the temperature, which is typical for slow chemical exchange or interconversion. Unfortunately, still lower temperatures are inaccessible because of the freezing point of DMF and the insolubility of the complex in other solvents such as CD$_2$Cl$_2$. Another observation is that H7 displays an upfield shift at lower temperatures, probably due to enhanced intermolecular $\pi\cdots\pi$ interactions that arise when molecules become less mobile.

In both investigations, the smaller shift of H2 compared with that of other protons may serve as a diagnostic criterion for the formation of closed structures in solution. It is also evident that the rapid exchange between the labile components continues down to to temperatures as low as −50 °C. Such dynamic behavior takes advantage of converting all thermodynamically disfavored intermediates into the most favored ones by a "self-correction" mechanism, provided that suitable solvent media are selected. The general conclusion reached by this comprehensive study of thermodynamically controlled self-assembly points out that cyclic structures are preferred over linear ones for enthalpic reasons, while small cycles are favored over large cycles (at low concentrations) for entropic reasons.[6a] Therefore, the exclusive formation of closed structures in our cases agrees with this conclusion because they all represent the smallest

topology possible for each specific combination of ligand and metal ions with predefined coordination geometries. Compounds **3** and **4** appear conflicting, but, when the fact that the Ag$^+$ ions adopt a different coordination geometry is taken into account, this can be understood. In the M$_2$L$_3$ cage, each Ag$^+$ ion possesses three bonds, one more than that in the M$_2$L$_2$ cage; however, the Ag−N bond distance decreases by about 0.16 Å from trigonal to linear coordination which may compensate for the loss of enthalpy on going from the trigonal prism to the metallacycle. In any case, the different distribution in a different solvent makes it easy to selectively crystallize the desired product from the corresponding "virtual combinatorial library".

Conclusion

A family of discrete nanoscopic molecular architectures with well-defined shapes and sizes, varying from two-dimensional macrocycles (**1**−**3**) to three-dimensional prismatic cages (**4**−**9**), has been prepared following a *ligand-directed symmetry-interaction* approach. The semirigid ditopic ligands **L^1**−**L^3** take on the *syn*-conformation[18] and act as an organic "molecular clip" to participate in the assembly by metal ions possessing C_n symmetry, yielding rectangular-shaped M$_2$L$_2$ metallacycles **1**−**3**, an M$_2$L$_3$ trigonal prism **4**, and M$_2$L$_4$ tetragonal prisms **5** and **6**. Similarly, the design of a tritopic ligand **L^4** which also adopts the *syn*-conformation[18] can lead to the formation of M$_3$L$_2$ trigonal prismatic cages **7**−**9** which represent the topologically identical but compositionally different counterparts of the M$_2$L$_3$ trigonal prism **4**, providing a complementary strategy for the construction of such structures. Different interior cavities were formed in which various types of guest molecules are accommodated: from spherical BF$_4^-$ and ClO$_4^-$ to rodlike CF$_3$SO$_3^-$; from neutral H$_2$O to negative I$^-$, and, most interestingly, to a flat, double-charged CuI$_3^{2-}$ guest complex. The diversity of the guest molecules endows the structures with tunable inclusion properties but also make it ambiguous for concluding that the assembly of the host molecules is induced by the anionic guests,[43] irrespective of the observation that no definite guest molecules are present in **1** and **2**. Outside the cages, there exist channels or voids generated by the large molecules, which are occupied by counteranions or solvent molecules. The solution structures have been established by combinatorial utilization of ^{1}H NMR and ESI-MS and were found to be consistent with the solid-state structures. The *in situ* reaction was monitored by ^{1}H NMR, including temperature-dependent NMR measurements, to provide solution dynamic information which indicates that the present molecular architectures are kinetically labile but thermodynamically stable. The virtual combinatorial library[37] is consequently expected to make it possible to predict preferential product formation for selective crystallization under specific conditions.[4c,6a,41] This indicates the existence of synthetically viable pathways to the rational design of discrete molecular architectures with comparatively low symmetry of a rectangular or prismatic shape.

(43) Johnson, D. W.; Raymond, K. N. *Supramol. Chem.* **2001**, *13*, 639.

Supporting Information Available: Selected bond distances (Å) and angles (deg). Space-filling modes of **1**−**7**, **9**·H₂O, and **9**·benzene·H₂O. Square channels extended along the *a* direction in **2**. 2D layers in **3**. X-ray crystallographic files in CIF format. This material is available free of charge via the Internet at http://pubs.acs.org.

JA034267K